Università Ca' Foscari - Venezia

DOTTORATO DI RICERCA IN

Science and Management of Climate Change

Scuola di dottorato in Global Change Science and Policy

Ciclo XXVII

Anno 2015

The role of the stratosphere on the multi-year predictability of the climate system

Settore Scientifico-disciplinare di afferenza: FIS/06

Tesi di dottorato di Miriam D'Errico, matricola 955952

Coordinatore del Dottorato

Prof. Carlo Barbante

Tutore del dottorando

Dr. Alessio Bellucci

Co-tutore del dottorando

Dr. Chiara Cagnazzo

Università
Ca'Foscari
Venezia

DOTTORATO DI RICERCA IN

SCIENCE AND MANAGEMENT OF CLIMATE CHANGE

Scuola di dottorato in Global Change Science and Policy

CICLO XXVII

Anno 2015

The role of the stratosphere on the multi-year predictability of the climate system

Settore Scientifico-disciplinare di afferenza: FIS/06

Tesi di dottorato di Miriam D'Errico, matricola 955952

Coordinatore del Dottorato
Prof. Carlo Barbante

Tutore del dottorando
Dr. Alessio Bellucci

Co-tutore del dottorando
Dr. Chiara Cagnazzo

To Anna & Francesco

Contents

1 Introduction **1**
- 1.1 Motivation . . . 1
- 1.2 Mechanisms of decadal variability . . . 2
  - 1.2.1 Sudden stratospheric warming . . . 2
  - 1.2.2 QBO and Holton-Tan relationship . . . 4
- 1.3 Objectives and Methodology . . . 6
  - 1.3.1 Decadal predictions framework . . . 6

2 Model description and experimental set-up **8**
- 2.1 Models description . . . 8
  - 2.1.1 The CMCC-CMS General Circulation Model . . . 8
  - 2.1.2 The MPI-ESM-MR Earth System Model . . . 9
- 2.2 Experimental setting . . . 9
  - 2.2.1 CMCC-CMS experiments . . . 9
  - 2.2.2 MPI-ESM-MR experiments . . . 10

3 Models evaluation **12**
- 3.1 Mean state and variability in the models . . . 12
  - 3.1.1 Surface temperature . . . 13
  - 3.1.2 Zonal mean zonal wind . . . 15
- 3.2 Predictive skill . . . 20
  - 3.2.1 Surface temperature . . . 22
  - 3.2.2 Zonal mean zonal wind . . . 28

4 Sources of predictability, stratospheric dynamics **36**
- 4.1 Sudden stratospheric warming . . . 36
  - 4.1.1 SSW detection method . . . 37
  - 4.1.2 Distribution of SSW events . . . 38
- 4.2 Holton-Tan relationship . . . 45
  - 4.2.1 Quasi-biennial oscillation Index . . . 46
  - 4.2.2 Composites . . . 46

5 Discussion and conclusions **50**

Bibliography **52**

Chapter 1

Introduction

1.1 Motivation

Within the wide set of timescales characterizing the climate variability spectrum, the interannual-to-decadal range bears the distinctive feature of being influenced by both natural and anthropogenic factors (Solomon et al., 2011). This is supported by an extensive list of observed examples of sustained (decadal-scale) climate variations with significant impacts on society, including changes in Atlantic hurricane activity (Latif and Keenlyside, 2011), temperature (see, e.g., Raible (2007)), precipitation (see, e.g., Hawcroft et al. 2012; Pfahl and Wernli 2012) and drought risk (Paredes et al., 2006). The ability of climate models to provide accurate climate forecasts over this specific range has been assessed in several studies. Earliest experiments based on realistically initialized climate models (Smith et al., 2007; Keenlyside et al., 2008; Pohlmann et al., 2009) paved the way to coordinated near-term (years to a few decades) prediction experiments performed as part of the Coupled Model Intercomparison Project Phase 5 (CMIP5; Taylor et al. (2012), Doblas-Reyes et al., 2013; Bellucci et al., 2014). These studies mainly focus on the role of ocean initialization, with a common result that there is some skill in decadal predictions, although differing over parameters, forecast times and region. In Hurrell et al.,(2009) is highlighted the strong dependency of near-term predictions on the dynamical model (Kim et al., 2012), the initialization strategy, and the reanalysis used to constrain the initial state of the model with a realistic representation of the climatic system. Several studies (Solomon et al., 2011; van Oldenborgh et al., 2012) indicate that a large part of predictive skill on multiannual to decadal timescales is associated with changes in the external forcing (anthropogenic greenhouse gases, aerosols, solar irradiance, and volcanic eruptions). Thus the decadal prediction is a joint initial-boundary value problem. For this reason the impact of initialization on predictive skill has to be critically examined comparing initialized simulations against uninitialised climate projections.
While the role of the ocean on decadal predictability has been extensively inspected (Meehl et al, 2009, 2013), so far little attention has been paid to the role played by other components of the climate system. This is partly motivated by the fact that the inherent timescale of atmospheric processes is generally considered to be too short to aid climate

prediction on seasonal to decadal timescales (e.g., Smith et al., 2012). However an exception of this general role is the memory of the tropical stratosphere (Scott and Haynes, 1998), exhibiting an interannual fluctuation of the zonal wind, a phenomenon known as Quasi-Biennial Oscillation (QBO)(Baldwin et al., 2001). Currently, only a few models attempt to fully represent stratospheric processes in the experimental frame of decadal predictions. Using high-top configurations of coupled ocean-atmosphere climate models with a well resolved stratosphere that have an internally generated QBO, Pohlmann et al. (2013) and Scaife et al. (2014) analysed seasonal and decadal forecasts to quantify the prediction skill associated with the QBO. They found some QBO predictability at the 4-year range but a weak QBO influence on the surface climate and predictability thereof. A connection between the QBO and the extra-tropical northern stratosphere, known as the Holton-Tan relationship (HTR) (Holton and Tan, 1980) relates the changes in the polar vortex strength and temperature to the QBO phase. Significant interannual stratospheric variability in the high latitudes of the northern hemisphere is also found and attributed to internal atmospheric variability, in relation to sudden stratospheric warming events in the extra-tropics (SSW; Butchart et al. 2000). The SSWs are defined when the polar vortex reverses its westerly zonal direction and turns to easterly (Charlton and Polvani, 2007b). SSWs are also relevant for their potential impact on the underlying troposphere, through stratosphere-troposphere coupling mechanisms (Baldwin and Dunkerton, 2001; Ambaum and Hoskins, 2002). Indications of a possible stratosphere-ocean connection occurring at inter-decadal timescales, through downward propagation of stratospheric circulation anomalies are also found (Reichler et al., 2012; Manzini et al., 2012). These multiple evidences of low-frequency variability in the climate system associated with stratospheric dynamics, suggest that the inclusion of a well-resolved stratosphere might be beneficial for improving the overall predictive ability of current climate models. An overview of the processes relevant for the decadal scale variability and predictability occurring in the stratosphere is provided in the following section.

1.2 Mechanisms of decadal variability

1.2.1 Sudden stratospheric warming

During winter in the northern polar stratosphere, variations in the strength of the vortex correspond to extreme 'polar vortex events' (Baldwin and Dunkerton, 2001) known as stratospheric sudden warming (Scherhag, 1952). SSW events occur when the winter stratospheric westerly wind reverses to easterly, causing a rapid rise in stratospheric temperatures over extreme northern latitudes (Matsuno, 1971; Andrews et al., 1987). Several studies have shown the downward propagation of SSW anomalies from the stratosphere to the troposphere (Baldwin and Dunkerton, 2001; Kodera and Koide, 1997, 1999). The anomaly originated in the upper stratosphere propagates downwards in the lower stratosphere where it is correlated with anomalies developing at the surface. Schimanke et al. (2011) found that a downward propagation of the stratospheric disturbance is significant on the troposphere before and after the occurrence of an extreme stratospheric event.

A downward atmosphere to ocean coupling could also exist, for example a link between low-frequency variations in the stratosphere and the Atlantic thermoaline circulation is studied by Reichler et al. (2012). Furthermore, Manzini et al. (2012) have documented the existence of inter-decadal variability in the stratosphere propagating to the ocean in the Northern Hemisphere winter in a CMIP5 pre-industrial simulation performed with the CMCC-CMS model. They suggest also that the northern stratospheric polar vortex anomalies propagate downward, related with the changes in the frequency of SSW events occurrence and driven by internal dynamical processes of the atmosphere-ocean system. This implies that intra-seasonal variations processes (Baldwin and Dunkerton, 2001) are also responsible for stratosphere-troposphere coupling at inter-decadal time scales. This leads to the hypothesis that in some cases stratospheric anomalies associated with SSW events, precursors of anomalies at the surface, could produce benefit for extended-range weather forecasts (Thompson et al., 2002; Baldwin et al., 2003). Thompson et al. (2002) and Scaife et al. (2008) discussed the potential predictability for NH extreme cold events observing the impact of the stratospheric circulation during pronounced SSW episodes in wintertime.

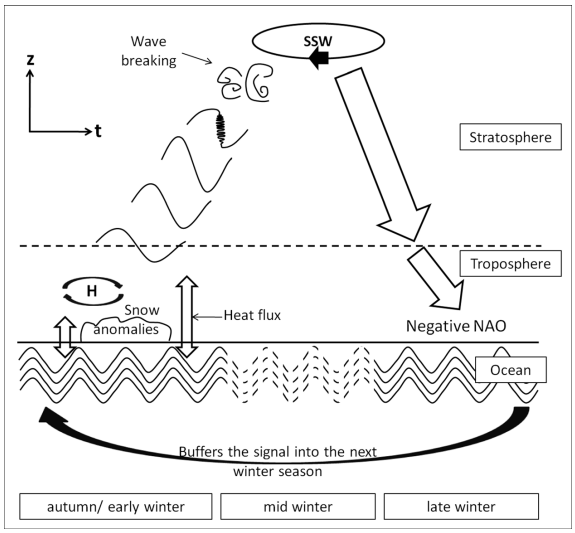

Figure 1.1: Schematic diagram outlining the mechanism behind decadal variability of SSW, as decribed in Schimanke et al. (2011) (Based on the works by Reichler et al. (2007) and Cohen et al. (2007)). For more detail see text.

Decadal variability is found in the extra-tropical northern hemispheric stratosphere (Butchart et al., 2000), attributed to the internal atmospheric variability and connected with a change in the frequency of sudden stratospheric warmings (SSWs), as external variability factors. Several other studies (Schimanke et al., 2011; Manzini et al., 2012) showed a significant multi-decadal variability in the frequency of extreme stratospheric events, evidence that both internal stratospheric climate variability and external stratospheric climate forcing can be important drivers of tropospheric climate (Reichler et al.,

2012; Manzini et al., 2012). In Figure 1.1 Schimanke et al. (2011) shows a mechanism for the multi-decadal variability in the number of SSWs, as an extension of the conceptual models of Reichler et al. (2007) and Cohen et al. (2007). They found significant coherence between the SSW frequency and parameters of the troposphere-surface system, such as snow cover anomalies that propagate upward from the troposphere to the stratosphere, decelerating the polar vortex (through wave dissipation and breaking). This stratospheric anomaly propagates downward causing a tropospheric response. In this way anomalies persist over an extended period and result in a multi-decadal variability of SSWs.

1.2.2 QBO and Holton-Tan relationship

A large inter-annual variability exists in the strength of the Northern stratospheric polar vortex in the extra-tropics. Variations of the polar vortex are influenced by external factors and by internal atmospheric dynamics (Charney and . Drazin, 1961; Matsuno, 1970; Plumb, 1985; Andrews et al., 1987). While the mechanisms of internal variability are not yet completely understood, a possible natural external factor of influence on the polar vortex variability include the quasi-biennial-oscillation (Baldwin et al., 2001) in equatorial zonal wind. The QBO is an east-west oscillation in stratospheric winds characterized by an irregular period averaging 28 months downward propagating, dominating the variability of the equatorial stratosphere. The QBO signature in zonal mean zonal wind in the tropical stratosphere has been widely analysed using different data sets (Angell and Korshover, 1962; Hamilton, 1984; Dunkerton and Delisi, 1985; Naujokat, 1986; Ortland et al., 1996).
Both modeling-based studies (Hampson and Haynes, 2006; Pascoe and Gray, 2006; Naito and Yoden, 2006; Kinnersley and Tung, 1999, 2010; Calvo et al., 2007; O'Sullivan and Young, 1992; Niwano and Takahashi, 1998) and reanalysis-based studies (Hu and Tung, 2002; Hitchman, 2002; Ruzmaikin et al., 2005; Garfinkel and Hartmann, 2007) have shown a robust effect of the QBO in the polar stratosphere.
The influence of the QBO on the extra-tropical northern stratosphere can be illustrated by the Holton-Tan relationship (HTR) (Holton and Tan, 1980). More specifically, Holton and Tan (1980) and numerous studies afterwards found that the northern stratospheric winter polar vortex is stronger (weaker) and colder (warmer) when the QBO measured at 50 hPa is westerly (easterly).
The HTR has been reproduced in simple models (Gray and Pyle, 1989; O'Sullivan and Salby, 1990; O'Sullivan and Young, 1992; Naito and Yoden, 2006), in atmospheric general circulation models with an imposed QBO and with a spontaneous QBO (Balachandran, 1995; Hamilton, 1998; Garfinkel et al., 2012; Anstey et al., 2010; Calvo et al., 2007), and in Chemistry Climate Models with an imposed QBO (Yamashita et al., 2011) and spontaneous QBO (Kinnersley and Tung, 2010). Therefore, the HTR is a robust feature, that is insensitive to the choice of the model and the representation of the QBO itself. Very recent studies on the CMIP5 coupled atmosphere-ocean models have also found that models with prescribed or spontaneously generated QBOs, showing realistic bimodal behaviour of the QBO and with a realistic strength of the variability of the vortex, report an HTR

that is generally weaker than in the reanalysis but with the right sign (Bo Christiansen, personal communication). Holton and Tan (1980) were the first to formulate a dynamical mechanism, suggesting that the QBO modulates the location of the sub-tropical critical wind line, thereby affecting the propagation of planetary waves into the stratosphere from the troposphere. Stationary planetary waves cannot propagate through easterly winds, their presence is therefore more confined in the NH middle to high latitudes when the equatorial winds are easterly, therefore leading to larger wave activity in these regions during the QBO easterly phase than in the westerly phase condition. Thus the polar vortex is more disturbed during the QBO easterly phase. Numerous studies have looked at the Eliassen-Palm (EP) fluxes, a measure of the direction and magnitude of planetary wave propagation (Andrews et al., 1987), and found that the extra tropical stratosphere EP flux is larger during QBO-E for November-January and less in March, also explaining the seasonality in the response. However, Kinnersley and Tung (2010) and Yamashita et al. (2011) found in observations and in a set of simulations performed with a chemistry climate model that EP flux in the lower stratosphere is directed more equator ward during QBO-E than QBO-W. Their explanation of the HTR implies a role for upper stratospheric winds; variations in the EP fluxes are associated with variations in the meridional circulation, therefore leading to adiabatic heating at 30N, strengthening the vortex during QBO-W by increasing the Equator to pole temperature gradient through the thermal wind relationship. There are also observational and modeling evidence for a role of the upper stratospheric winds and wind shear on the HTR mechanism, and this could be important for understanding the observed modulation of the HTR by the 11-yr solar cycle (Karin, 2005; Camp and Tung, 2007). To summarize, there is a consensus that winds at the Equator influence the polar vortex through a modulation of the NH planetary wave flux, however a debate still exists on the role of equatorial upper stratospheric winds and the QBO-associated meridional circulation. However we have to bear in mind that the response to planetary wave forcing is likely to be non linear, and this means that observations and different models cannot be easily compared, because if for example a model may be able to correctly simulate the equatorial wind influence on the propagation to planetary waves, it may predict an incorrect strength of HTR due to a bias in the climatological wave forcing or to a bias in the climatology of the vortex itself. The role of the non linear interaction between QBO and El Niño/Southern Oscillation (ENSO)(McPhaden and Co-authors, 1998; Wang and Picaut, 2004) on the polar vortex will be briefly discussed when comparing results between the MPI and CMCC models (see Chapter 4).

The interest for possible connections between the QBO and the extra-tropical troposphere is not only determined by the dynamics that may connect these regions but also the potential role that such relation might have on climate predictability (Boer and Hamilton, 2008). Seasonal forecasting is difficult in the extra-tropics since the predictable signal is small compared to unpredictable natural variability noise (see Barnston et al., 1999; Goddard et al., 2001). Boer and Hamilton (2008) state that although the additional skill is modest, the result supports the contention that taking account of the QBO could improve extra-tropical seasonal forecasting skill. Using seasonal forecasts Marshall and

Scaife (2009) suggested that realistic simulation of the QBO in an atmospheric GCM should improve multiannual forecasting of European surface winter up to several years due to the multi-annual predictability of the QBO. However in the more recent study of Scaife et al. (2014) although the QBO presents a good degree of predictability up to three years in a group of state-of-the-art coupled atmosphere-ocean models that are used for performing decadal predictions, its signal to the winter surface is small.

1.3 Objectives and Methodology

The aim of this study is to examine the decadal variability and predictability of the climate system, associated with processes occurring in the stratosphere. We base our analysis on a set of near-term predictions performed with state-of-the-art stratosphere-resolving climate models, initialized with an estimated state of the ocean and atmosphere. In order to fully establish the impact of realistic model initialization, results from decadal integrations are contrasted against a twin set of historical, non-initialized, climate projections covering the same time period. The set of hindcasts used are based on the CMCC-CMS and MPI-ESM-MR coupled models. These two systems differ in the adopted initialization procedure, with the CMCC-CMS model being initialized in the ocean only, while MPI-ESM-MR model is initialized in both atmosphere and ocean. The different initialization of the model components makes it possible an analysis of the individual effects associated with atmosphere and ocean. Understanding the role played by the stratosphere on decadal scale climate predictability is a topic which has received relatively little attention, so far. Here, the decadal predictability associated with the occurrence of SSWs in the extra-tropical stratosphere, and a possible role of QBO on extra-tropical predictability will be examined through the novel approach represented by decadal predictions.
Details on the decadal prediction experimental framework are provided in the following section.

1.3.1 Decadal predictions framework

The near-term decadal predictions are a very new attempt to fill the gap between intraseasonal to interannual time scales and century-long climate projections (Pohlmann et al. 2009; Meehl et al., 2009; 2013). These new type of integrations are initialised with an estimate of the observed system and carried forward for about 10-30 years. The decadal predictions are performed in retrospective (hindcast), referred to initialized predictions of past cases, and forecast mode. The CMIP5 protocol recommended a minimum of 3 ensemble members for 10 year hindcasts initialized from observed climate states near the years 1960 to 2005 every 5 year. The benefit of this technique is to reduce the unpredictable noise and the observational uncertainty through initialization (Goddard et al., 2012). The decadal prediction experiments intend to reproduce natural low-frequency climate variability as well as climate change through external forcing (Goddard et al.,

2012; Smith et al., 2012). The state of initialization should therefore well represent the climate state at the start date (Pohlmann et al., 2009). Depending on the initialization strategy (full field or anomaly initialization) a bias might emerge, when the equilibrium state of the model does not coincides perfectly with the real climate state (Meehl et al., 2013). The full field initialization implies that the initial model state is replaced by constraining model values close to observed state. After initialization the model drifts from the initial state to the models preferred equilibrium state (Meehl et al., 2009; Goddard et al., 2012). In the anomaly initialization the observed anomalies are added to the model climatology (Meehl et al., 2009; Goddard et al., 2012) and the use of this scheme avoids the main problems with drift in the climate predictions (Pohlmann et al., 2009).
The ensemble members are taken from one model or from multiple models to form a multi-model ensemble. An ensemble of initial conditions is typically generated in order to investigate the climate sensitivity to the small perturbations in the initial state (Du et al., 2012). Different methodologies or variations on those methods for perturbation may be utilized to generate ensemble, by resulting from different philosophical approaches to the ensemble generation problem (Meehl et al., 2013).
The verification of hindcasts is essential for predictions to improve errors in initialization strategies, model initialization of natural variability and model responses to external forcing. The principle of forecasting is always associated with a given forecasting "lead time", the latter indicating the time interval between the start date and the future time at which the value must be evaluated. Measures of the success of a prediction quality (also referred to as predictive skill) of the hindcasts is evaluated for different averaging periods at different forecast times. These can illustrate the quality of the information throughout the period of the hindcast and the skill dependence on averaging and lead time. Additional details on the decadal predictions are explained in chapters 2 and 3.

Chapter 2

Model description and experimental set-up

In this chapter we provide a description of the high-top CMCC-CMS and MPI-ESM-MR climate models used in this work, and the details of the decadal prediction experiments. Decadal integrations are performed following the CMIP5 protocol for near-term predictions (Taylor et al., 2012), as part of the Intergovernmental Panel on Climate Change (IPCC) Fifth Assessment Report (AR5).

2.1 Models description

2.1.1 The CMCC-CMS General Circulation Model

The CMCC-CMS model is a stratosphere-resolving coupled ocean-atmosphere model, developed at the Euro-Mediterranean Center on Climate Change (CMCC-CMS)(Manzini et al., 2006; Giorgetta et al., 2006; Cagnazzo et al., 2007). The atmospheric component is ECHAM5 (Roeckner et al., 2003) with a well-resolved stratosphere; it has a high vertical resolution (95 levels) and a horizontal resolution of T63 (about 1.9 x 1.9 deg). The model internally reproduces the QBO in the equatorial stratosphere (Giorgetta et al., 2006). The incorporation of the resolved stratospheric component implies the use of the middle atmosphere version (Manzini et al., 2006) of the atmospheric model in the coupled system. The middle atmosphere version has its top at 80 km (0.01 hPa) and includes the parametrization of momentum conserving orographic and non-orographic gravity wave drag (Hines, 1997). The ocean component is the OPA8.2 model (Madec et al., 1998) in the ORCA2 global configuration, solving primitive equations on a tripolar horizontal grid, with 2 poles in the Northern Hemisphere. The resolution is 2°x 2°L31 with a meridional refinement near the Equator approaching a minimum 0.5°grid spacing. The ocean model does also include the Louvain-La-Neuve (LIM) model for the dynamics and thermodynamics of sea-ice (Fichefet and Morales-Maqueda, 1999). Atmosphere and ocean are coupled by OASIS3 coupler (Valcke, 2006) and the coupling methodology and implementation is described in (Fogli et al., 2009).

2.1.2 The MPI-ESM-MR Earth System Model

The MPI-ESM-MR model is a stratosphere-resolving Earth-system model developed at the Max Planck Institute Earth System Model in the mixed resolution MPI-ESM-MR. The atmosphere model is ECHAM6 atmospheric GCM (Stevens et al., 2013) the successor of ECHAM5 (Roeckner et al., 2003, 2006). The most significant differences between ECHAM5 and ECHAM6 (T63) concern the radiation schemes, the computation of surface albedo, and the triggering condition for convection. The vertical resolution of 95 levels (L95) allows the generation of a quasi-biennial oscillation (QBO) in the equatorial stratosphere. Details on the features of the QBO generated in the ECHAM6 GCM can be found in Krismer et al. (2013). The ocean component is the Max Planck Institute Ocean Model (MPIOM; Jungclaus et al., 2006; 2013) with horizontal grid spacing of the ocean from nominally 1.5°to 0.4°. This ocean grid is a tripolar quasi-isotropic grid with two northern poles in Siberia and Canada and the third pole at the South Pole. The ocean biogeochemistry is represented by the HAMOCC model (Ilyina et al., 2013), while JSBACH (Raddatz et al., 2007) was used as the land surface component. The vegetation cover as well as land-surface albedo are evaluated in Brovkin et al. (2013). The different components of the model are coupled via the OASIS3 (Valcke, 2006).

2.2 Experimental setting

2.2.1 CMCC-CMS experiments

A set of decadal prediction experiments are performed for the 1960-2005 period. No volcanic aerosols effect is included in the model forcing. The decadal predictions consist of 3-member ensembles of 10-year simulations starting in January 1961 at 5-year intervals (Fig. 2.1). Model initialization is done via a full-value procedure (Pierce et al., 2004; Smith et al., 2013) from three different ocean reanalysis and applied to the ocean state only, the sea-ice is initialized through a model climatology, while the atmospheric initial states are derived from a control simulation performed with historical twentieth century radiative forcing conditions. The ocean initial states are provided by an ensemble of ocean reanalysis, differing by assimilation methods and assimilated data (Bellucci et al., 2013), performed using the same ocean model configuration (ORCA2) used in the coupled system. A single-member historical simulation for the same time period of the predictions using identical forcing conditions is used as the non-initialized control integration.

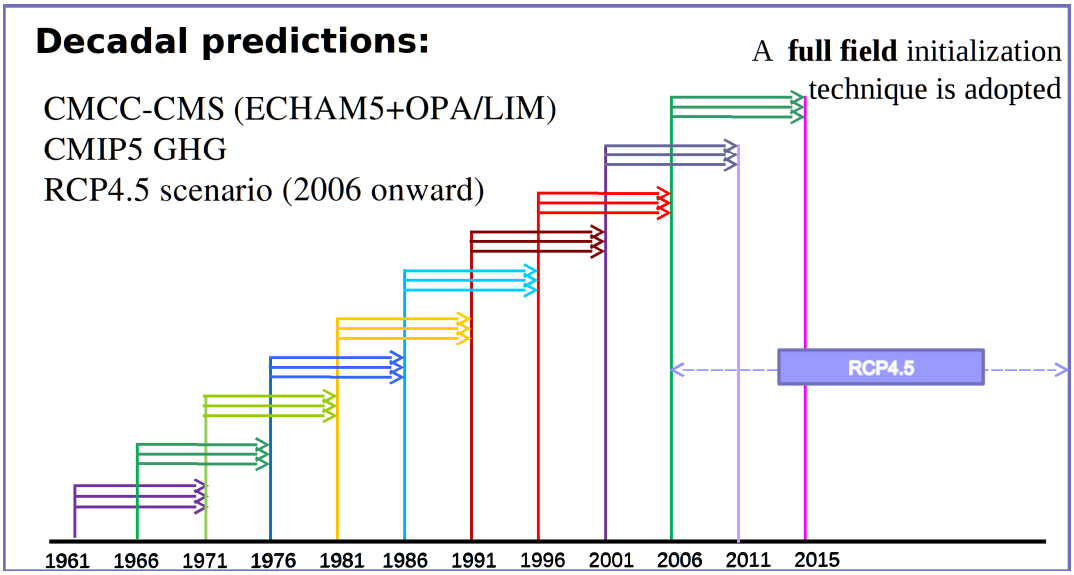

Figure 2.1: Schematic illustration of the experimental setup for CMCC-CMS decadal runs.

2.2.2 MPI-ESM-MR experiments

The experimental setting used by the Max Planck Institute is summarized in Figure 2.2. In this study we analyse 3 ensemble members of decadal hindcasts (Pohlmann et al., 2013).

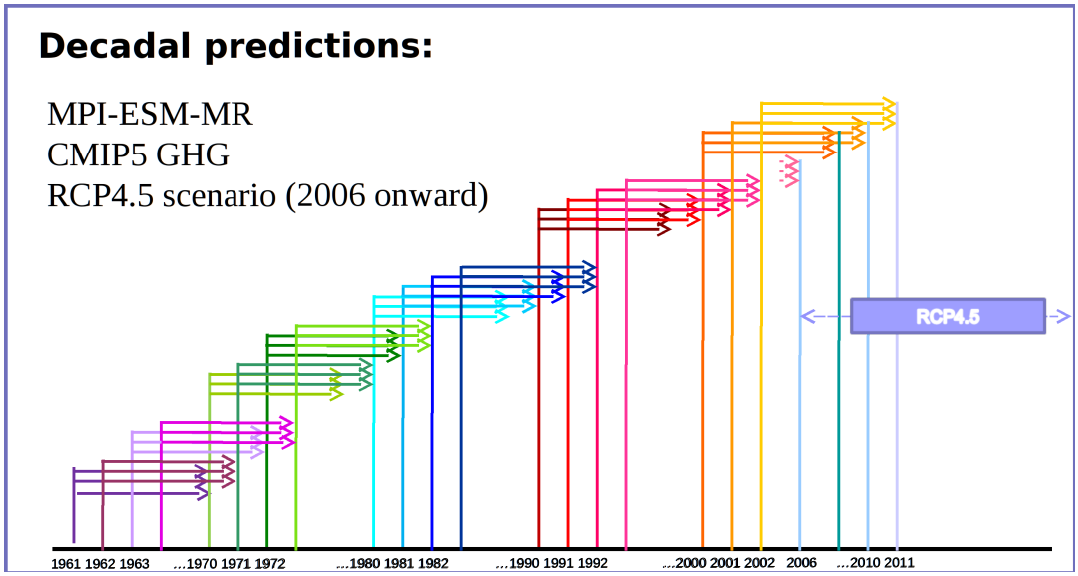

Figure 2.2: Schematic illustration of the experimental setup for MPI-ESM-MR decadal runs.

The hindcasts are initialized every year between 1961 to 2012. The oceanic component is initialized with temperature and salinity anomalies from the ocean reanalysis system 4 (ORAS4) from ECMWF (Balmaseda et al., 2012), through anomaly initialization. The atmospheric component is initialized with full-field technique with data from ERA-40 Re-Analysis for the period 1960-1989 and ERA-Interim (Dee et al., 2011) for the period 1990-2005, respectively. A corresponding set of three-member uninitialized historical simulations are used as control integration.

Chapter 3

Models evaluation

In this chapter, the ability of the models used throughout this work (CMCC-CMS, MPI-ESM-MR) in reproducing the observed long-term climatology and interannual (and longer) variability is assessed by comparing results from historical simulations and observations/reanalyses. Also, the predictive skill of decadal hindcasts performed with the afore mentioned models is evaluated through appropriate statistical metrics.
Climate variability on interannual time scale appears to arise from interactions of ocean and atmosphere. In order to understand the climate variability, the variability of both systems is needed to be studied. The time scales of the variability of these two components, ocean and atmosphere, are very different. In particular, the atmosphere exhibits rapid adjustments to changes for short and medium-range weather forecasts, while slow variations in SST provide a source of potential predictability for climate fluctuations from interannual to decade time scales. This natural variability of the climate system is here assessed together with the ability of the model to simulate it. We examine the surface temperature that play a key role in regulating the ocean circulation and its interaction with the atmosphere. The most fundamental descriptor of the atmospheric general circulation is the zonal mean zonal wind distribution. It is analysed the annual and zonal mean values of the zonal wind and its interannual and interseaonal variability. A common approach to quantifying the magnitude and spatial distribution of surface temperatures and ZMZW variability is to map the standard deviation of annual and seasonal mean fields.

3.1 Mean state and variability in the models

In the following sections the annual mean and its standard deviation of surface temperatures and ZMZW are shown for CMCC-CMS and MPI-ESM-MR historical simulations. For the surface temperatures the set of observations is of Hadley Centre Global Sea Ice and Sea Surface Temperature (HadISST) (Rayner et al., 2003) over the years 1961-2013. For the ZMZW ECMWF Re-Analysis (ERA)-40 (Uppala, 2005) over the period of 1962-2002.

3.1.1 Surface temperature

The SST is a variable widely used as a proxy to describe ocean circulation patterns. It also has an important role in climate science as a key indicator of variability. In Figure 3.1 both models have the SSTs mean distribution in agreement with the observed (Fig. 3.1a,c,e).

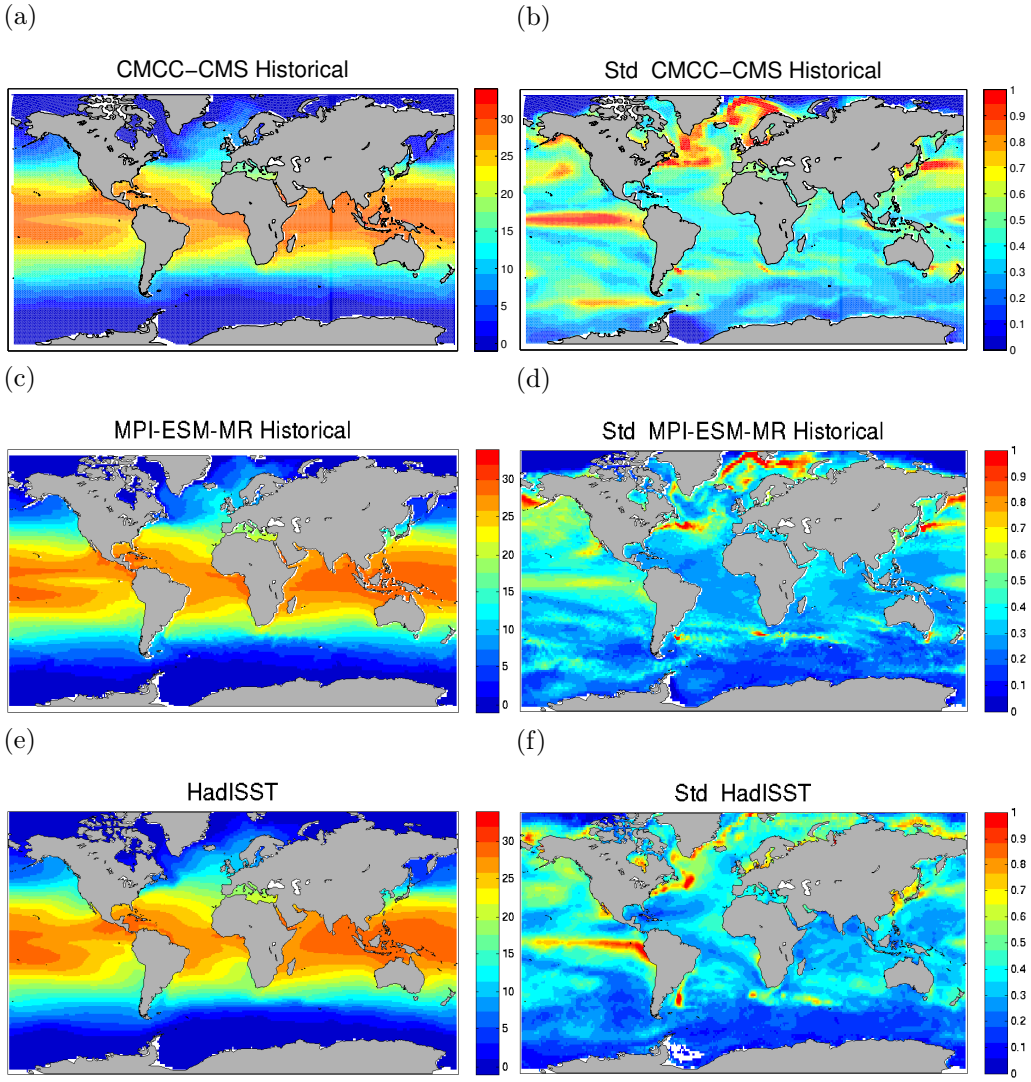

Figure 3.1: Annual mean sea surface temperature (°C) (left column) and standard deviation (right column) (°C) for a);b) CMCC-CMS; c);d) MPI-ESM-MR historical simulations; e);f) HadIsst observations.

The SST variability appears well-represented in spatio-temporal patterns (Fig. 3.1b,d,f) as in the eastern to central equatorial Pacific that corresponds to the region governed

by the ENSO interannual variability mode. This is the area featuring the largest SST anomalies at interannual scale. Both models tend to exhibit an overly westward extended Cold Tongue in the equatorial Pacific. Other two regions show high variability, the western-boundary current regions of the Kuroshio and the Gulf Stream. The upwelling regions in the tropical Atlantic and the eastern Pacific in both models are weaker showing warmer water compared with observations. In general the SST variability is higher in the CMCC-CMS simulations (3.1b) compared with MPI-ESM-MR and observations, more specifically in the northern North Atlantic (subpolar basin), in the equatorial Pacific (ENSO driven region) and North Pacific. The variability of the Cold Tongue region is underestimated by the MPI-ESM-MR model which is important for the coupled feedbacks of the ENSO variations as the interaction between ENSO and QBO that may affect the polar vortex changes (discussed in Ch. 4). The interannual variability over land areas of the surface temperature is also analysed for both models. In Figure 3.2 the mean and standard deviation of 2-metre temperature (T2M) (over land) together with SST for CMCC-CMS simulations and of the air temperature for MPI-ESM-MR runs are compared with the combined sea surface temperature and land surface air temperature compiled by the Hadley Centre and the Climatic Research Unit (HadCRUT3, Brohan et al., 2006). For this comparison both SSTs and T2M fields are linearly interpolated over the HadCRUT3 grid for CMCC-CMS model. The same interpolation is applied to the air temperature field for MPI-ESM-MR model. In Figure 3.2a,c,e the mean surface temperature pattern shows a broad agreement with the observations for both models. From the standard deviation patterns is visible that the CMCC-CMS severely underestimates the interannual surface temperature variability over land, particularly over the North American and Eurasian continents. A more evident underestimation of the land surface temperature variability together with the Cold Tongue region is shown in the standard deviation of MPI-ESM-MR model.

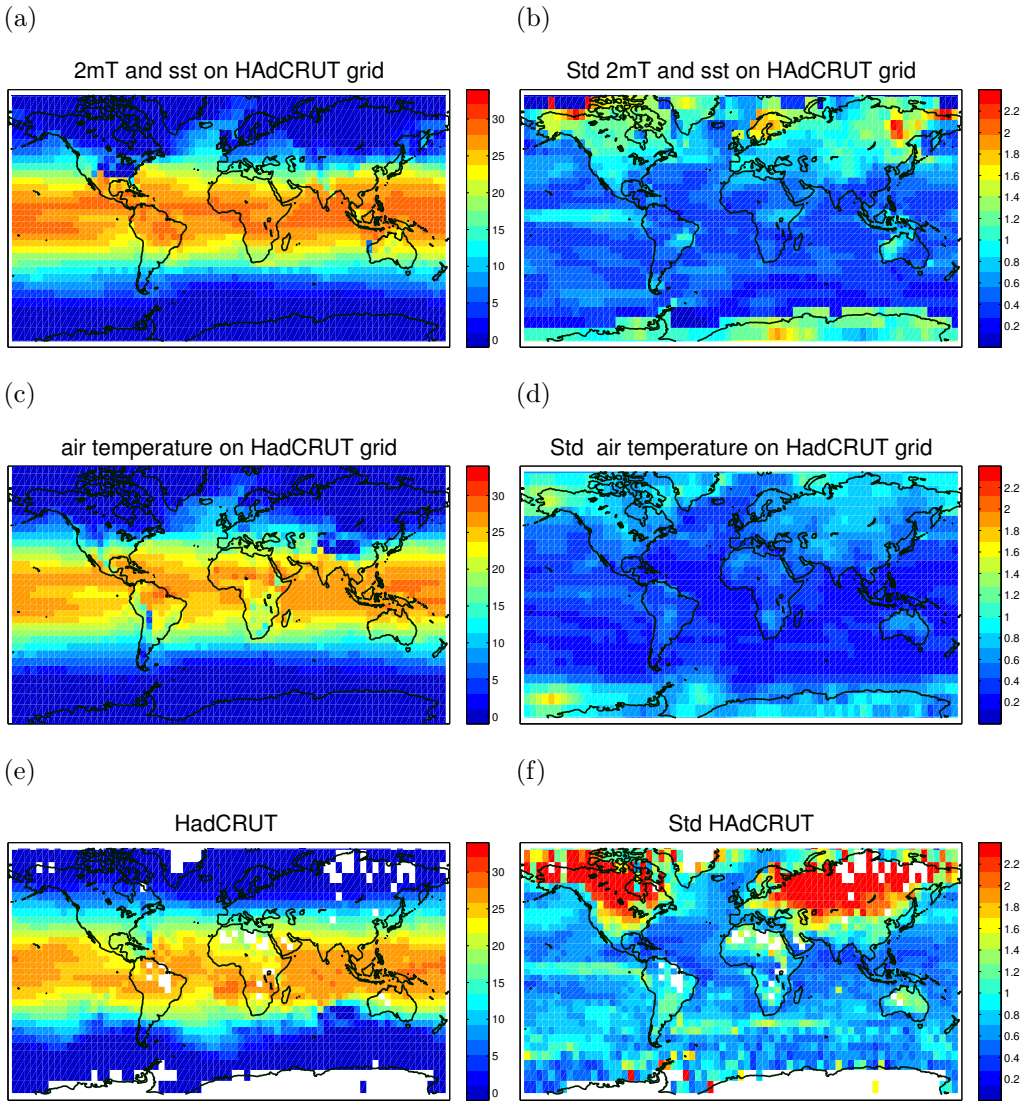

Figure 3.2: Annual mean surface temperatures (°C) (left) and standard deviation (°C) (right) for a);b) CMCC-CMS simulations; c);d) MPI-ESM-MR simulations; e);f) HadCRUT observations.

3.1.2 Zonal mean zonal wind

In this section, we assess the annual mean and NH winter (JFM) zonal mean zonal wind (ZMZW) in both models to corresponding mean of the reanalysis. We focus in the troposphere-stratosphere regions.
The simulated annual mean winds show similar structure compared to the reanalysis (Fig. 3.3). Prominent features are cores of strong westerly winds in middle latitudes at

200hPa level. The westerlies are stronger extending until upper stratosphere in South Hemisphere while in opposite hemisphere the westerlies are weaker. The equatorial lower stratospheric zone is dominated by zonally symmetric regimes of alternately easterly and westerly winds above 100 hPa to the higher stratosphere with maximum amplitude near 10 hPa. This equatorial lower stratospheric phenomenon is known as Quasi Biennial Oscillation. As we see in Figure 3.3b,d,f the standard deviation has the highest value in the tropical stratosphere in both models with similar patterns of the variability observed.
The zonal mean zonal winds averaged over JFM is shown in 3.4 for the CMCC-CMS and MPI-ESM-MR historical simulations and show a realistic structure in the two hemispheres. The 60N jet is stronger and has a larger interannual variability in the MPI-ESM-MR models, in the CMCC-CMS model winds do not reach 20 m/s between 50 and 10 hPa. The QBO is most evident in the zonal wind near equatorial stratospheric region with strong easterlies in SH. The winter variability of the QBO is high together with an other variability featured by changes in high latitude in the troposphere-lower stratosphere. Compared to MPI-ESM-MR and observations, CMCC-CMS display a less regular phase and a reduced vertical extent of the QBO signal (see Fig. 3.5). On the other hand, both CMCC-CMS and MPI-ESM-MR largely overestimate the observed QBO amplitude, specially above 20 hPa, as also documented in Manzini et al. (2012) for CMCC-CMS and in Giorgetta et al., (2013) for MPI-EM-MR.
A time-height cross-section of the monthly-mean zonal-mean zonal wind over the equator (10S-10N) is shown in Figure 3.5 for the two historical model simulations and reanalysis. It is not expected that the observed time series is reproduced, as the QBO time series in the model simulations can be in arbitrary phase. We examine the frequency, the amplitude and the vertical structure typical of the QBO. In both models, the period of the oscillation is about 28 months, in good agreement with reanalysis.
However, both the westerly and the easterly phases are less regular in CMCC-CMS compared with MPI-ESM-MR alternation which shows also westerly phases at lower altitudes as it is in the reanalysis. MPI-ESM-MR has a more realistic distribution of the QBO period, however, largely overestimates the QBO amplitude above 20 hPa (see Manzini et al., 2012), CMCC-CMS and Giorgetta et al., (2013), MPI-EM-MR). Here we do only a partial analysis of the QBO, for more details see Krismer et al. (2013).

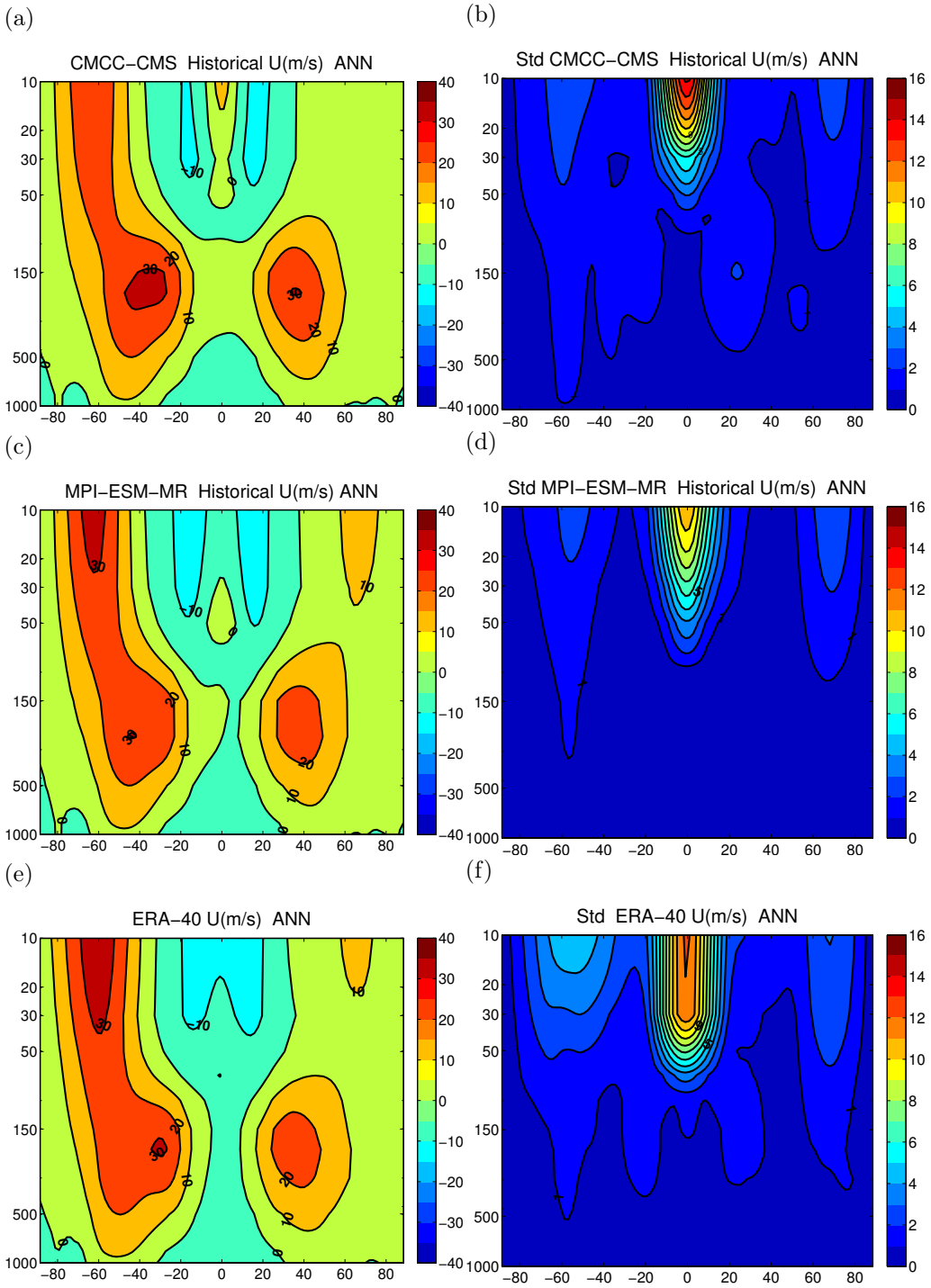

Figure 3.3: Annual mean of ZMZW (left column) (m/s) and standard deviation (right column) (m/s) for a);b) CMCC-CMS; c);d) MPI-ESM-MR historical simulations; e);f) ERA-40 resnalysis.

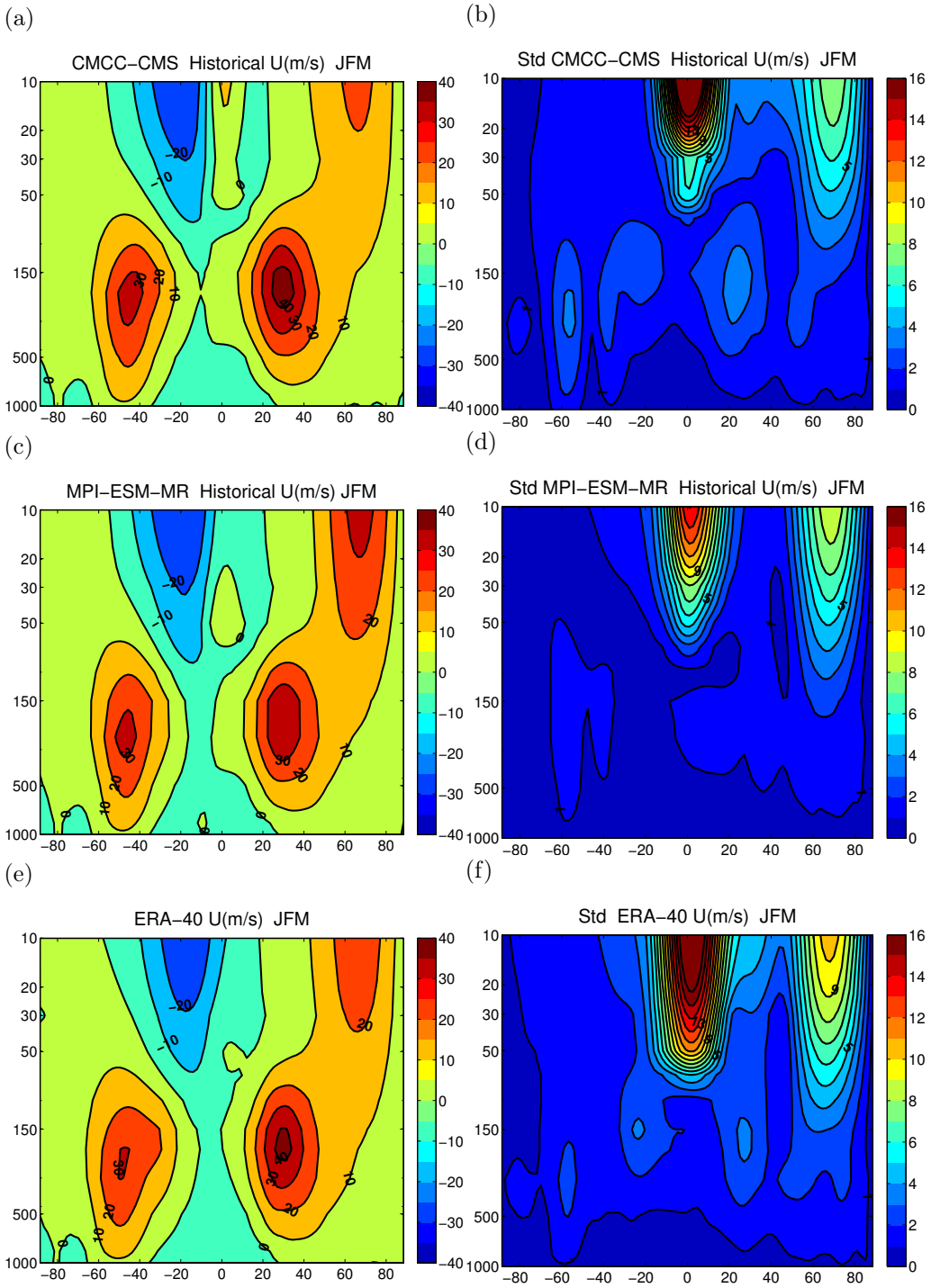

Figure 3.4: mean over JFM of ZMZW (left column) (m/s) and standard deviation (right column) (m/s) for a);b) CMCC-CMS; c);d) MPI-ESM-MR historical simulations; e);f) ERA-40 resnalysis.

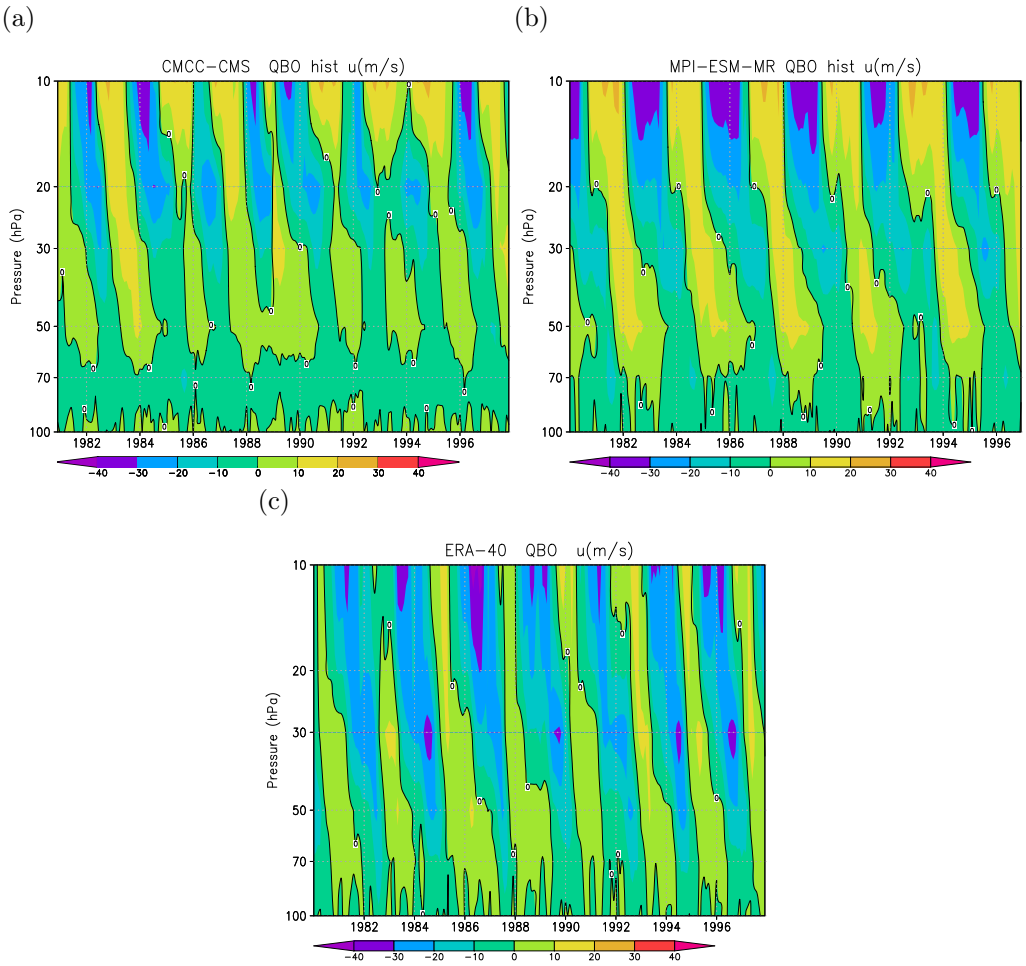

Figure 3.5: Yearly period of zonal mean zonal winds averaged over the equatorial region (10S-10N) (m/s) from single realizations for historical simulations of a) CMCC-CMS; b) MPI-ESM-MR; c) ERA-40 resnalysis.

Summarising, both models have the mean surface temperature and ZMZW similar to the observed. However some difference is found in the variability, as the lack of SSTs variability in the tropical Pacific and of surface temperature variability over land in MPI-ESM-MR model. The MPI-ESM-MR model has larger interannual variability of the jet than CMCC-CMS and displays a more regular phase of the QBO, whose amplitude is overestimated.
To quantify the quality of predictions a verification of the hindcast skill may be performed in a variety of ways including correlation or mean square error (e.g., Goddard et al. 2012). These methods are detailed in the following section.

3.2 Predictive skill

The choice of the verification metrics is made in way to answers specific questions regarding the quality of the forecast information. For example, verification metrics can identify errors or biases in the forecasts and drive to a more effective use of them. The questions address the accuracy in the forecast information and the representativeness of the forecast ensembles to indicate forecast uncertainty.
In this study we focus mainly in two questions, what is the magnitude of the probability forecast errors and whether the initial conditions initialization in the hindcasts lead to more accurate predictions of the climate.
The forecast quality might be verified correlating forecast with the observations. The direct correlation may be influenced by systematic errors of forecast, when the models are initialized with state close to the observations. In dynamical forecasting the model mean-climate evolution during the forecast time may drift towards its own mean state, leading to a long-term adjustment. This drift depends on the time of the forecast, especially in the case of the full-field initialization. To correct this drift and an associated initial shock of the system, a drift is removed to the model data by subtracting the average forecast from the individual raw initialized hindcasts.
In Figure 3.6 we applied this procedure to the global weighted area averaged SSTs of CMCC-CMS simulations. The SSTs of forecast-hindcast shown in yellow scale curves (1961-2015) are drift removed and they are well fitted with the observations (black line). In gray line the SSTs for uninitialized run are also shown. Comparing forecast with historical SSTs, the initialization influence is highlighted.

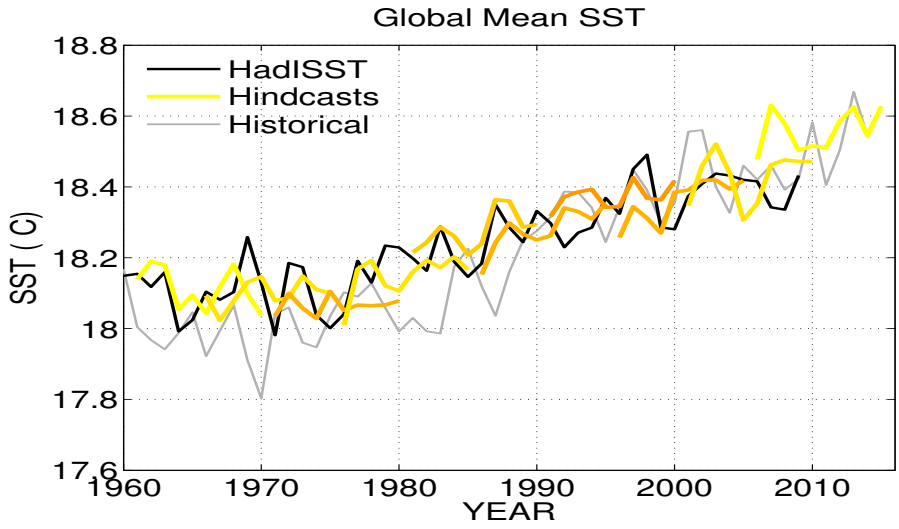

Figure 3.6: Global annual-mean area weighted surface temperature anomalies (relative to 1961-2015) initialized hindcasts (yellow scale colr curves)are compared with equivalent uninitialized simulations (gray curves), and with observations (black curve) from HadISST (1960-2009).

The temporal evolution of drift appears to be model and variable dependent and the importance of drift should be assessed based on the application. In many circumstances, such as anomaly initialization (Smith et al., 2013; Keenlyside et al., 2008; Pohlmann et al., 2009; Matei et al., 2013), drift may be negligible. Adjustment time scale of the atmosphere is fast and the drift signal may be small. For the MPI-ESM-MR model drift correction we refer to Kruschke et al. (2014) paper.
For consistency in all of the performed analyses, all variables (both ocean and atmospheric) have been bias corrected following the method outlined in (CMIP-WGCM-WGSIP, 2011). Therefore the correlation is calculated over the anomalies according to the anomaly correlation coefficient (ACC) in equation 3.1 (Jolliffe and Stephenson, 2003; Wilks, 2006a). The ACC is one of the most widely used measures in the verification of spatial fields and it is also adopted by the international community following the Global Data-processing and Forecasting System (GDPFS) of the World Meteorological Organization (WMO, 2010, 2012):

$$ACC(\tau) = \frac{\sum_{i=1}^{N} h'_{\tau i} o'_{\tau i}}{\sqrt{\sum_{i=1}^{N} \left(h'_{\tau i}\right)^2 \sum_{i=1}^{N} \left(o'_{\tau i}\right)^2}} \tag{3.1}$$

$$\text{where} \quad h'_{\tau i} = h_{\tau i} - \overline{h_\tau} \quad \text{and} \quad o'_{\tau i} = o_{\tau i} - \overline{o_\tau}. \tag{3.2}$$

The $h'_{\tau i}$ and $o'_{\tau i}$ terms represent the forecast and observed anomalies, the over-bar is time average and N the number of available data along the start date dimension for a given forecast time τ. The anomaly time-series have been computed by subtracting an estimate of the corresponding climatology at each forecast time, representing the departures of specific forecasts from its normal state. The correlation coefficients are calculated over the ensemble mean for the hindcasts of each model.
The ACC can be regarded as a skill index measuring of the success of a prediction against observationally based information. Following the recommendations from Goddard et al. (2013) the predictive skill is evaluated through analysis of the ACC over 2-5, 6-9 lead years average for both observations and forecast and at lead time 1. The 2-5 and 6-9 lead-time averages represent the interannual time scales, excluding the first year of the prediction, as it represents overlap with seasonal-to-interannual predictions, and the imprint of initial observed conditions is strong. The year 2-5 average still represents the interannual timescale, but it discards the influence from initial conditions, it is likely still dominated by year-to-year variability and less by the climate change signal as it is for 6-9 average. The ACC score always ranges from -1.0 to 1.0. If the forecast is perfect, the score of ACC equals to 1.0, i.e. larger ACC corresponds to a better skill. For a given lead time period, the ACC is calculated over 10 values (one for each start date) for CMCC-CMS, for MPI-ESM-MR 5-yearly initialized forecasts and over 52 for MPI-ESM-MR yearly initialized forecasts.
The model prediction skill is examined by comparing with the observation, the annual mean of the sea surface temperature, of the 2-meter temperature, and of the zonal mean

zonal wind (ZMZW, see section 3.3.2) for initialized and uninitialized simulations of each model. Another important measure of skill is based on the mean squared error (MSE, 3.3), used in order to assess whether the initialization of the hindcasts leads to more accurate predictions with respect to an uninitialized simulation. The Mean Square Skill Score (MSSS) is a deterministic metric (Murphy, 1988) which measures the improvement of the probabilistic forecast relative to a reference forecast (uninitialized climate simulation). The MSSS, based on the mean squared error (MSE) is defined as follows:

$$MSE\tau = \frac{1}{N}\sum_{i=1}^{N}[h'_{\tau i} - o'_{\tau i}]^2 \tag{3.3}$$

$$MSSS\tau = 1 - \frac{MSE}{MSEref} \tag{3.4}$$

The Mean Squared Skill Score (MSSS) is defined as one minus the ratio of the squared error of the forecasts (MSE) to the squared error for reference forecast ($MSEref$) in this case the set of uninitialized hindcasts (3.4). The MSE is always positive. However the MSSS may have negative values, if the forecast error is larger than that of the uninitialized run. A positive value for the MSSS indicates that the forecast is more accurate than the uninitialized run. The MSSS is unity for a perfect forecast, and zero if the forecast is undistinguishable from uninitialized simulation. The MSSS here represents the fractional improvement, or degradation, of the initialized hindcasts over the uninitialized reference. Here as reference uninitialized forecast we use the historical run divided in the same time segment as hindcasts. We diagnose the MSSS for the SSTs in the CMCC-CMS model considering a 4 year mean separately at near-term (2-5 lead time) and long-term (6-9 lead time) hindcasts (WMO, 2012). For MPI-ESM-MR model the calculation of MSSS and 2-metre temperature ACC we mention Goddard et al. (2013) reference.

3.2.1 Surface temperature

In this section we evaluate the predictive skill of the annual mean surface temperatures in CMCC-CMS hindcasts for the period 1960-2010, through the ACC (3.1). The ACC is computed at different lead times, i.e. 2-5 lead time and 6-9 lead time. The reference observation data set used in this section for ACC calculation is HadISST (Rayner et al., 2003). Prior to the computation of anomaly correlation, both model and observation were linearly interpolated onto a common grid, in that case over HadISST grid. In the end of the section we give an overview of the ACC of the annual mean SSTs for the MPI-ESM-MR decadal simulations. A one-sided Student t-test is used to verify statistical significance of the correlations, dependent on sample size which varies with reference dataset. Furthermore, serial correlations were taken into account by adjusting the effective sample size according to:

$$N' = N\frac{(1 - r_{1,x}r_{1,y})}{(1 + r_{1,x}r_{1,y})} \tag{3.5}$$

where $r_{1,x}$ and $r_{1,y}$ are the first-order autocorrelation coefficients of time series x and y, and the where N and N'are the original and effective sample sizes respectively and ρ_1 is the lag-1 autocorrelation coefficient. Based on this test at 95% statistical significance is reached for ACC higer than 0.6 (marked with white spots, over red regions). In order to have a general view on the influence of a well-resolved stratosphere on the predictive skill, we compare the ACC from CMCC-CMS hindcasts against a reference set of decadal simulations, performed with a low-top configuration of the CMCC model (CMCC-CM; Bellucci et al. (2013), 2014). It is important to remark that the low-top model configuration has a different horizontal resolution (T159L31), but the same ocean model (OPA8.2, L31).

In Figure 3.7ab the predictive skill of the SSTs in the low-top model are shown at 2-5 and 6-9 lead years (see Bellucci et al., 2013, Fig. 3). The red color in the palette represents the high correlation and then a high skill. Bellucci et al. (2013) found higher correlation over the Indian Ocean, over the sub-tropical North and South Atlantic, and over the western North Pacific at 2-5 lead time. Moreover the predictive skill is larger at 6-9 lead-years over the same regions.

We show here in Figure 3.7cd the difference in the ACC of SSTs between high top and low top hindcast runs (Fig. 3.8ab, at both near-long terms. Qualitatively the difference shows a high value in South Pacific ocean and in tropical South Atlantic at 2-5 lead time, while at 6-9 lead time a positive correlation is located in the North and extra-tropical Pacific. These results are supported in previous forecast experiments which suggest that tropospheric skill is enhanced when the forecast model top extends to the stratosphere (Baldwin et al., 2003; Charlton and O'Neill, 2003; Christiansen, 2005; Kuroda, 2008; Marshall and Scaife, 2010). The low-frequency energy contained in the stratosphere seems to be capable to affect the SSTs through the propagating anomalies from the stratosphere downward to the ocean, as can be the SSW occurrence changes (Manzini et al., 2012), or to the deeper ocean, as the thermoaline circulation (Reichler et al., 2012).

More information are given by the global average area weighted of the ACCs in Figure 3.7e. Globally the high top model has a higher skill (about 0.33 and 0.39 at 2-5 and 6-9 lead time respectively), compared with the 0.27 (at 2-5) and 0.33 (at 6-9) of the low top model. Both models however show a better global skill when the average is made over long term lead time. This may be related to the effect of boundary forcing dominating over the initialization in the longer (6-9 years) term, as at longer time scales the influence of the initial conditions decreases and the importance of the forcing increases. This is a robust feature of current climate models, found in both single and multi-model studies (Bellucci et al., 2013, 2014).

Succeeding, we evaluate the effect of initialization through the analyses of the ACC and MSSS of the SSTs in the initialized hindcasts compared to the uninitialized run over the same period. Focusing on the high top CMCC-CMS model, Figures 3.8ab display the ACC of hindcasted SSTs at 2-5 and 6-9 lead years.

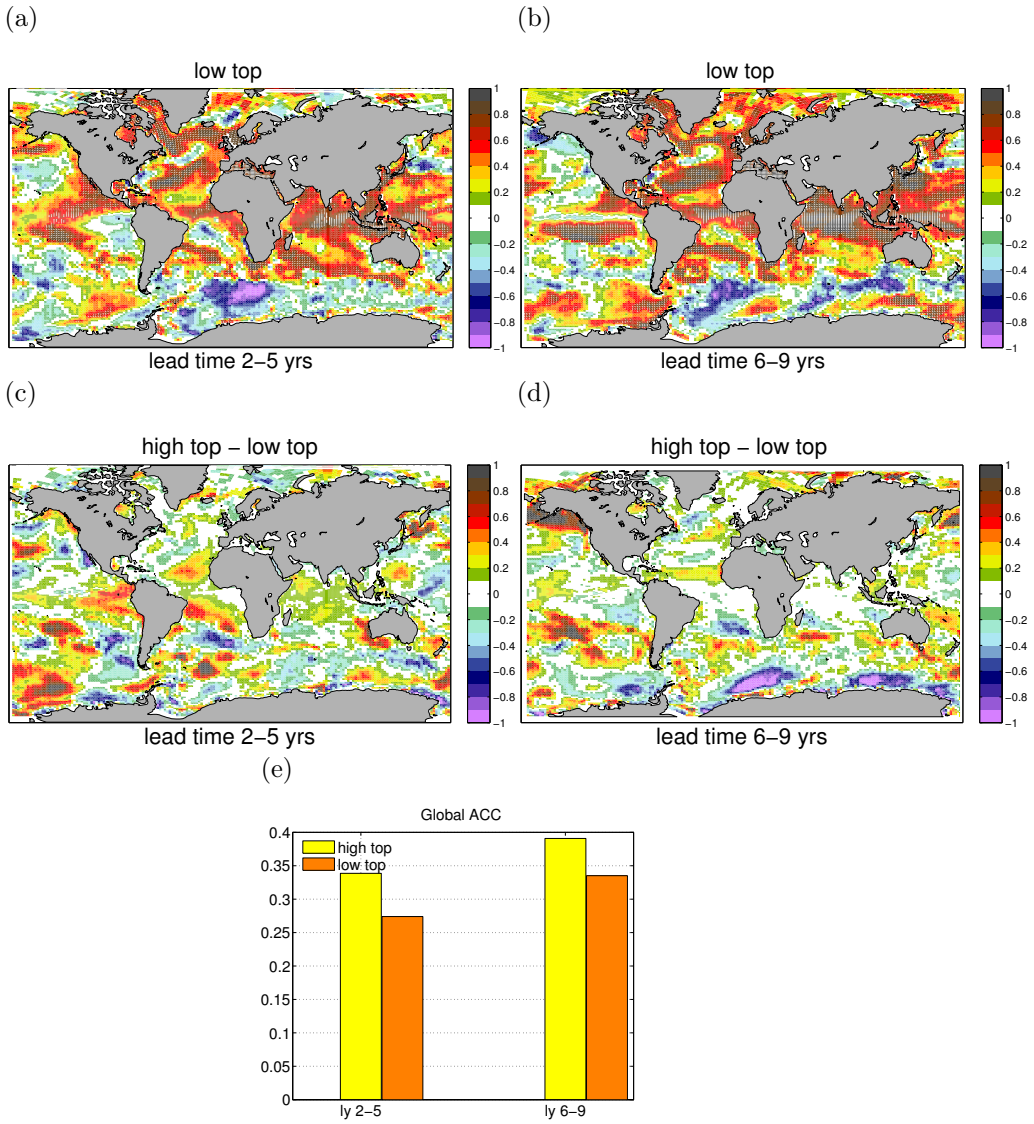

Figure 3.7: ACC of SST for Low-top model for lead-years 2-5 (a) and 6-9 (b). Correlations larger than 0.6 are statistically significant at the 95 % level according to a one-sided Student's t-test (white spots); Difference of anomaly correlation coefficient of SST hindcasts between Low-top and Hight-top models for years 2-5 (c) and 6-9 (d); Globally averaged for ACC of CMCC-CMS model (yallow bar) and of CMCC-CM (orange bar)(e).

In the near term (2-5 years) statistically significant skill is found over vast portions of world oceans, in particular the equatorial Indian Ocean, tropical pacific and the North Atlantic (white spots over red regions). Areas characterized by negative ACC values are also found mainly in the Southern Hemisphere. A qualitative similar pattern is found in the 6-9 lead -years term but with even wider regions featuring significant predictive skill, specially over the Indo-Pacific sector.

The verification of the skill due to ocean initialization is evaluated comparing the SST ACC of initialized hindcasts against the historical run (3.8cd).

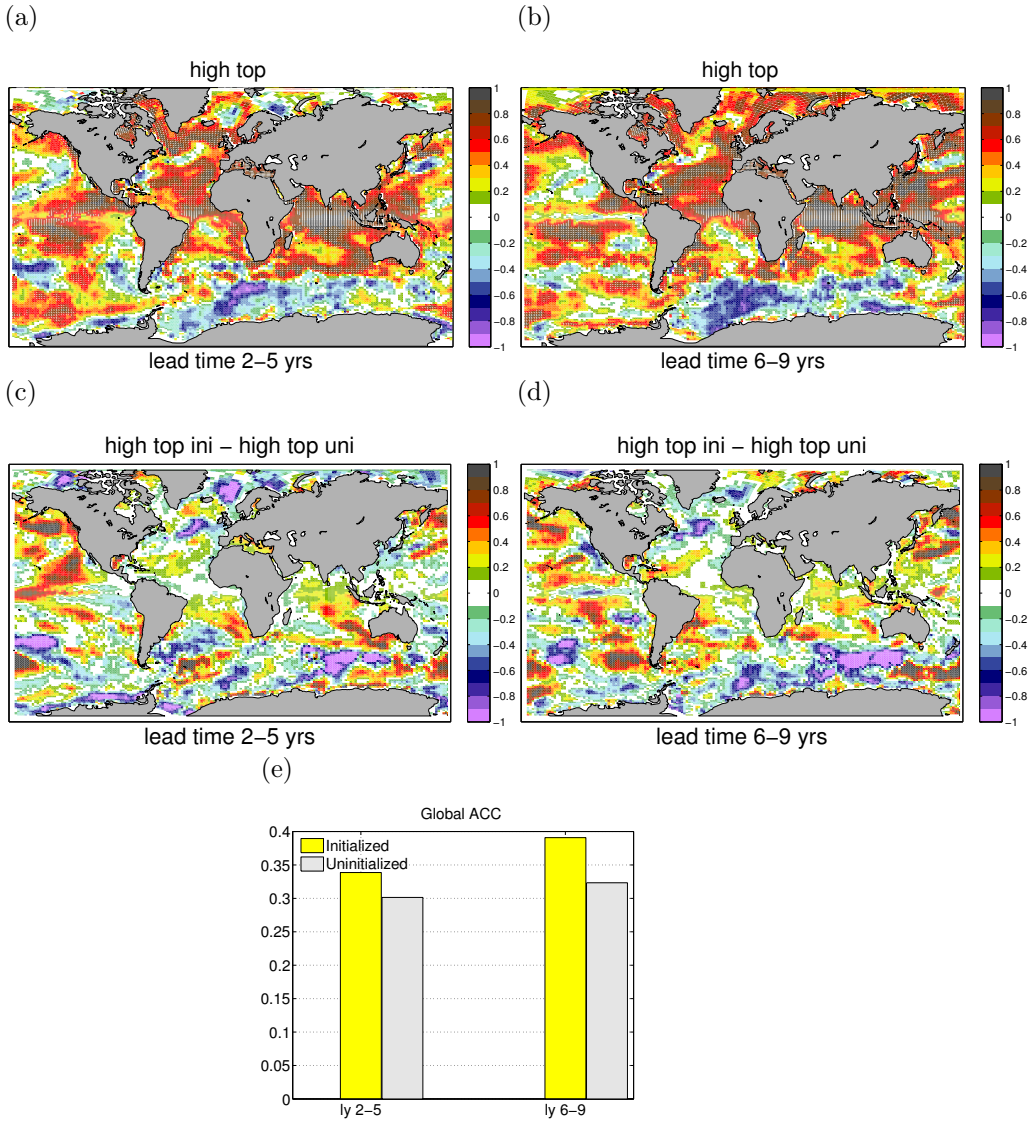

Figure 3.8: ACC of SST for high-top model (CMCC-CMS) for lead-years 2-5 (a) and 6-9 (b). Correlations larger than 0.6 are statistically significant at the 95 % level according to a one-sided Student's t-test (white spots); Difference of anomaly correlation coefficient of SST hindcasts between initialized and uninitialized hight-top model for years 2-5 (c) and 6-9 (d); Globally averaged for ACC initialized (yallow bar) and of uninitialized (gray bar)(e) simulations.

Notice here the red color means initialized is "better than" uninitialized. From this comparison, a better skill of the initialized runs over North and extra-tropical Pacific,

near to the North-West coast figures out at 2-5 lead-years, while at longer term hindcast an enhanced skill is found over North, tropical and South Pacific. Over the Indian Ocean region in both lead-year intervals, the skill difference shows an added value from initialization. The high skill of the SSTs in the Indian Ocean can be largely attributed to the effect of the varying radiative forcings and partly attributed to aerosols from volcanic eruptions(Guemas et al., 2013). The global mean skill (3.8e) reveals a systematic improvement initializing the system.

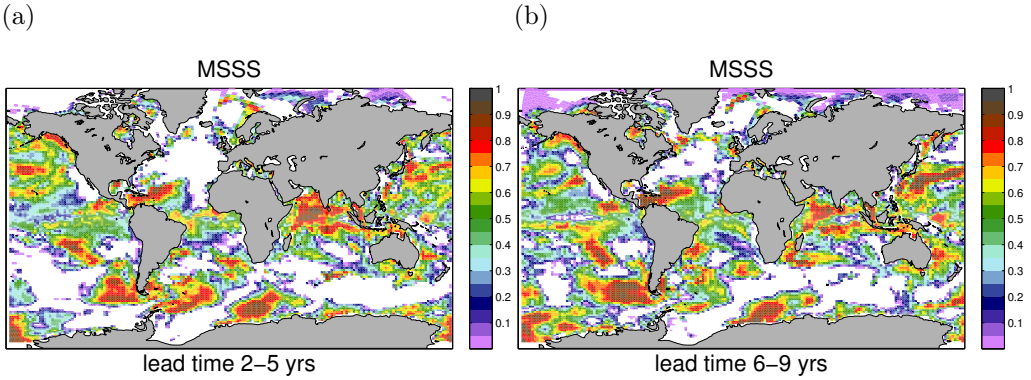

Figure 3.9: Mean squared skill score (MSSS) evaluated for SSTs (CMCC-CMS model). A historical uninitialized simulation spanning the same period of the predictions, and identical forcing conditions has been used as a reference hindcast. Negative values are shown in white.

Information about initialization effects on the accuracy of the forecast is given by MSSS verification metric. In Figure 3.9 the skill score is positive over Indian Ocean, most of Pacific and South Atlantic regions for both near and long term lead times.

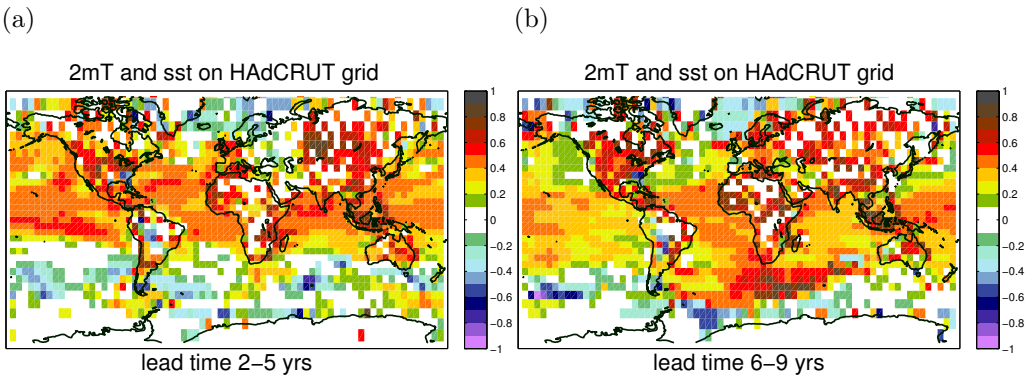

Figure 3.10: ACC of 2-m temperature (CMCC-CMS model) for years 2-5 (a) and 6-9 (b)with CRUTEM3 data set; merged ACC of SSTs with ACC of 2-m temperature in respect to the HadCRUT3 for years 2-5 (c) and 6-9 (d).

Negative MSSS are found over in large areas of the Southern Ocean as well as in

the North Atlantic ocean highlighting the regions where the initialization does not give an improvement with respect to the historical. From a comparison of the MSSS with the ACC differences of the SSTs in Figure 3.8cd, it is visible a correspondence between regions featuring negative anomaly correlations and negative MSSS (see in particular the Souther Ocean).
In order to analyse the predictive skill over the land areas for the decadal hindcasts, the ACC is designed for the global 2-m temperature with respect to HadCRUT3 observations, over HadCRUT3 grid.

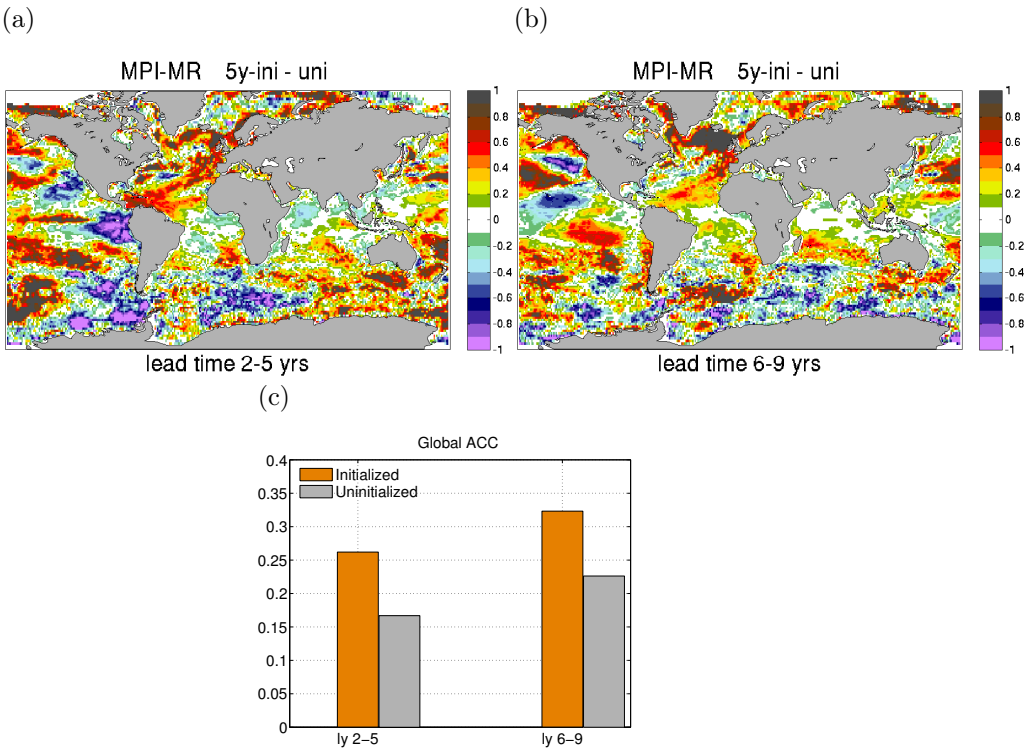

Figure 3.11: Difference of anomaly correlation coefficient of SST hindcasts between initialized and uninitialized MPI-ESM-MR model for years 2-5 (a) and 6-9 (b),(Matei et al. 2013, in preparation); Globally averaged for ACC initialized (orange bar) and of uninitialized (gray bar)(c) simulations.

The ACC maps are computed merging the ACC of initialized SSTs hincasts over ocean with the ACC of 2m temperature over land, at 2.5 and 6-9 lead year (Fig. 3.10cd). Enhanced skill is found in longer term over most of the continental regions. Over central Africa continent the positive correlation is visible and equal in both term time, however in the Eurasia and North America at 6-9 lead time the predictive skill increases.
In order to give an overview about the MPI-ESM-MR SSTs predictive skill, in Figure 3.11ab the ACC of SST differences for initialized and uninitialized hindcasts are displayed. A better skill for initialized simulation are located over North Atlantic, in

tropical regions, North Pacific and Southern Ocean at 6-9 lead year. Also the evaluation of the globally averaged ACC of the SSTs confirms that in the longer term the correlation is higher compared with near term at 2-5 lead time (from Matei et al. 2013, manuscript in preparation). The initialization in both models give globally an enhanced skill of the SSTs which is higher for longer term lead time, compared with historical runs. Regionally there is a general agreement between the models, with exception for the North Atlantic Ocean that shows an higher skill in the MPI-ESM-MR model.

3.2.2 Zonal mean zonal wind

In the previous section we evaluated the predictive skill associated with typical variables (SST and 2-metre temperature) characterizing the Earth surface climate. Here we assess the skill associated with the ZMZW in the troposphere and the stratosphere.
The correlation is computed over annual averaged ensemble mean value at lead-year 1, 2-5 and 6-9, for equally sub-sampled predictions and reanalysis. ERA40 is used as reference reanalysis to evaluate the correlations. A one-sided Student's t-test is used to verify statistical significance, assuming meaningless negative correlations, significant at 95% level those larger than 0.6. For better understanding the initialization effects the ACC difference between initialized and uninitialized run are analysed, equivalent to the method of removing local tendencies from both observations and model results, before computing anomaly correlations. The applied methodology of comparing initialized against uninitialized simulations is to be preferred to the detrending procedure as the latter is subjected to the limitation of assuming linearity of the trend.
Figures 3.12a-b shows the ACC at lead-year 1 for CMCC-CMS hindcasts. There is a gradual increment in the overall skill with lead time, particularly pronounced in the NH troposphere. Enhanced skill is located in low stratosphere sub-tropical regions reaching the surface in Northern hemisphere (NH) area (Fig. 3.12a). The 6-9 ACCs (Fig. 3.12e-f) are high over large region compared with lead year 1. On the decadal time scale, one may conclude that this is the evidence of skill driven by initial and boundary condition confirmed by the difference ACC plots that show added value on the skill by the initialized hindcasts at lead-year 1 and 6-9. In equatorial stratospheric region the ACC displays no-skill at lead year 1. This concur with the fact that the atmosphere is not initialized (Fig. 3.12a) in CMCC-CMS model. A largest improvements in the predictive skill of the hindcasts, compared to the historical simulations, are fond in the NH (Fig. 3.12, left column) and even though the atmosphere is not initialized there is large predictability in the polar NH stratosphere.
Next the ACC for ZMZW in the 5-yearly initialized MPI-ESM-MR system is described (Fig. 3.13). Here the effect of the atmosphere initialization is evident, especially in the equatorial stratosphere where the QBO is active (see section 3.1).

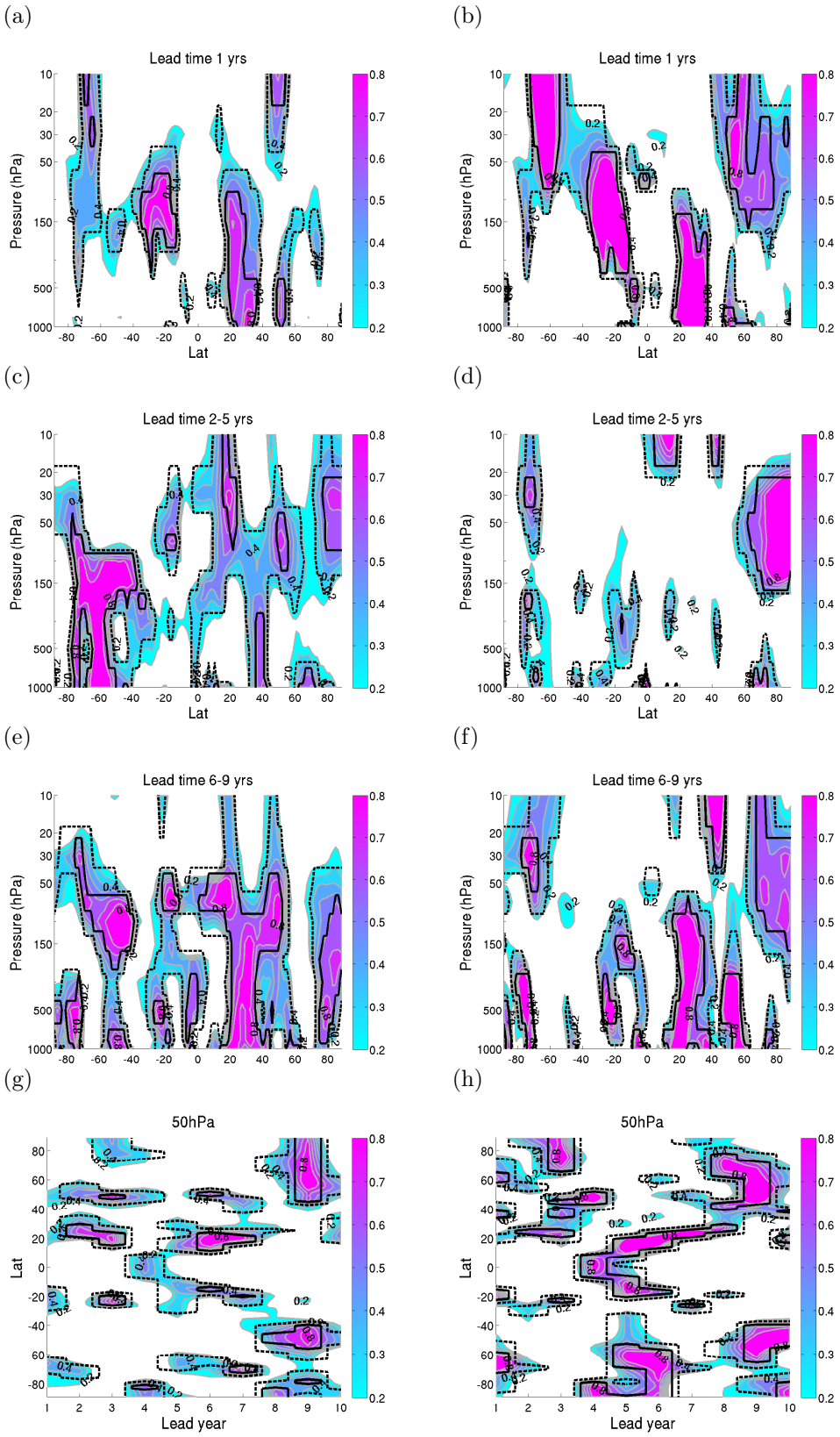

Figure 3.12: ACC of ZMZW hindcasts (left column), differences of initialized minus uninitialized hindcasts (right column); at lead time 1 (a, b); at lead time 2-5 (c,d); at lead time 6-9 (e,f); cross section latitude-lead-year at 50hPa (g,h). Correlation larger than 0.6 are significant at 95% level (solid black line), those larger significant than 0.4 are at 80% level (dashed black line), for CMCC-CMS model.

The gradual decrease of ACC in the tropical stratosphere with lead-time strongly suggests that the QBO is predictable up to 2-5 years. A similarly high skill region is found in the extra-tropics around 50 N and 50 S, highly coherent along the vertical, from surface to stratosphere. The skill in the extra-tropics shows an even longer persistence, compared with the equatorial stratosphere, with significant correlations up to lead-years 6-9. Comparing initialized with uninitialized simulations reveals that initialization has a positive impact on the skill in the areas affected by the QBO /polar vortex connection. This result is found also in the ACC computed for the yearly initialized hindcasts.
Overall there is a strong consistence between the ACC patterns emerged in the 5-yearly hindcasts and those emerging in the yearly case. Indeed in Figure 3.14 skill of yearly initialized hindcasts has a similar ACC compared with 5-year initialized runs, however the skill is shown with a lower statistical significance. In the specific in Figure 3.14g,h the stratospheric equatorial skill is high after 4 year from initialization, a time range longer than the weather forecasts associated with initial atmospheric state. In agreement with the high skill in QBO zone till lead time 4, the recent study of Pohlmann et al. (2013), with the same model and similar experimental setup (5 ensemble-members, 1 year initialized MPI-ESM-MR, MiKlip forecasts), shows a significant predictive skill related to the QBO of up to 4 years. In a recent study based on UK Met Office and MiKlip decadal hindcasts Scaife et al. (2014) demonstrates predictability of the QBO extending more than 3 years, although they found that it does not guarantee predictability of QBO effects on the surface during winter in decadal climate prediction.
At lead-year 1 the high skill in QBO and NH polar vortex region is clear and it is still visible and wide at lead time 2-5 (Fig. 3.14a) with 80% of significance. As before, a small area and low skill are left at lead time 6-9. A link between these two high skill zones at near term prediction may be explained by the Holton and Tan relationship (Holton and Tan, 1980) that connects the QBO phase with variations of the north-polar vortex strength. This relationship is studied as predictable source in the stratosphere in section 4.2. Studies as Garfinkel and Hartmann (2007) and Calvo et al. (2009) show a possible modulation of the HTR by the ENSO. This may add a possible influence by the ocean initialization on the HTR in the initialized hindcasts.
An interesting result is given by the latitude-lead time cross section of the ACC at 50hPa (Fig. 3.14g,h). The correlation at 50N-50hPa along each lead time is higher at lead time 1 and 5 (0.4). This result will be analysed in the end of this section in Figure 3.16.
The lower significance shown by yearly initialized compared with 5-yearly initialization leads to think about the existence of sub-sampling error. Due to the quasi-biennial phase of the QBO, one may wonder whether, by initializing every 5-years the same phase of the QBO is systematically sampled.

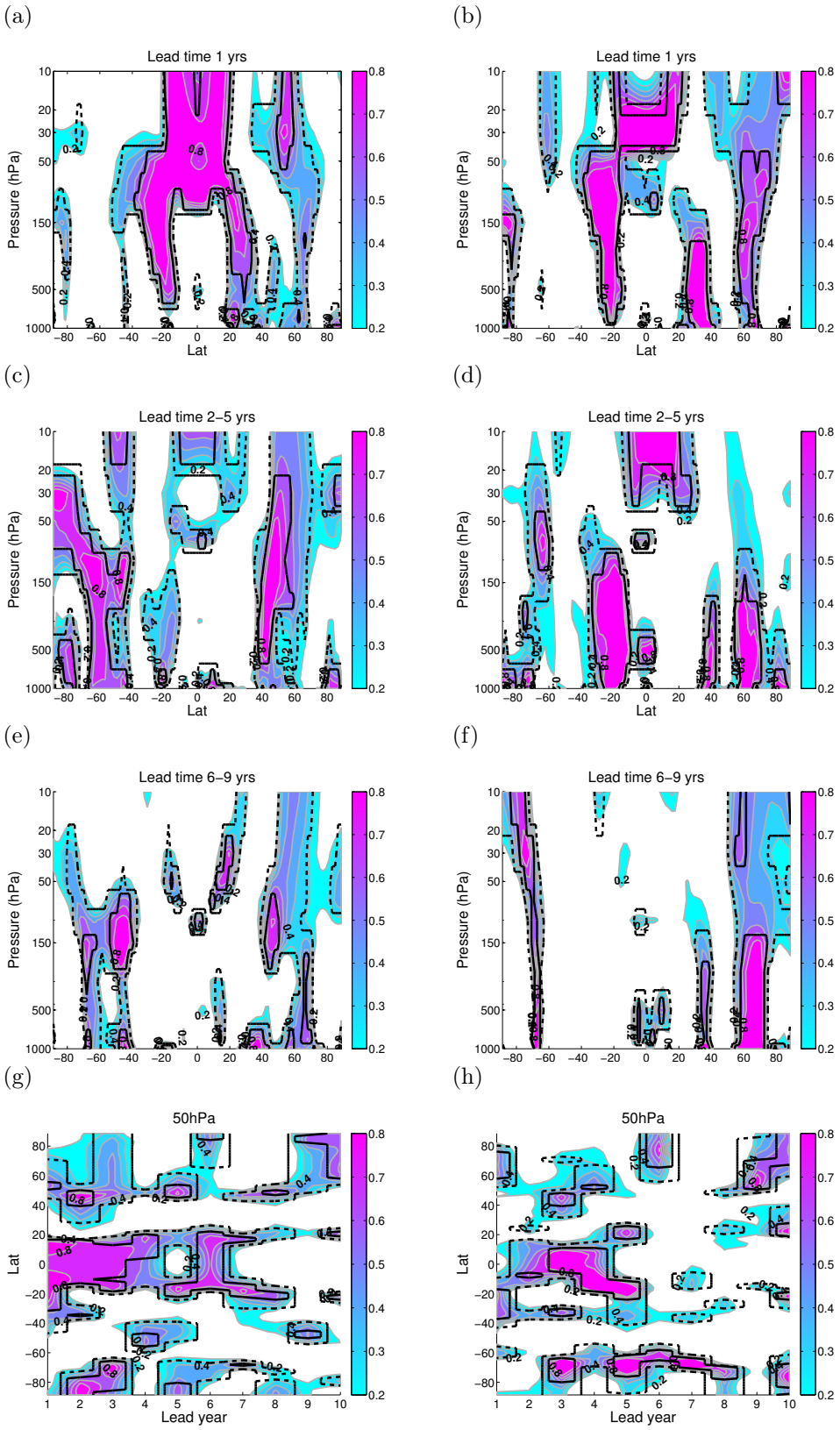

Figure 3.13: ACC of ZMZW hindcasts (left column), differences of initialized minus uninitialized hindcasts (right column); at lead time 1 (a, b); at lead time 2-5 (c,d); at lead time 6-9 (e,f); cross section latitude-lead-year at 50hPa (g,h). Correlation larger than 0.6 are significant at 95% level (solid black line), those larger significant than 0.4 are at 80% level (dashed black line), for MPI-ESM-MR every 5 year initialized.

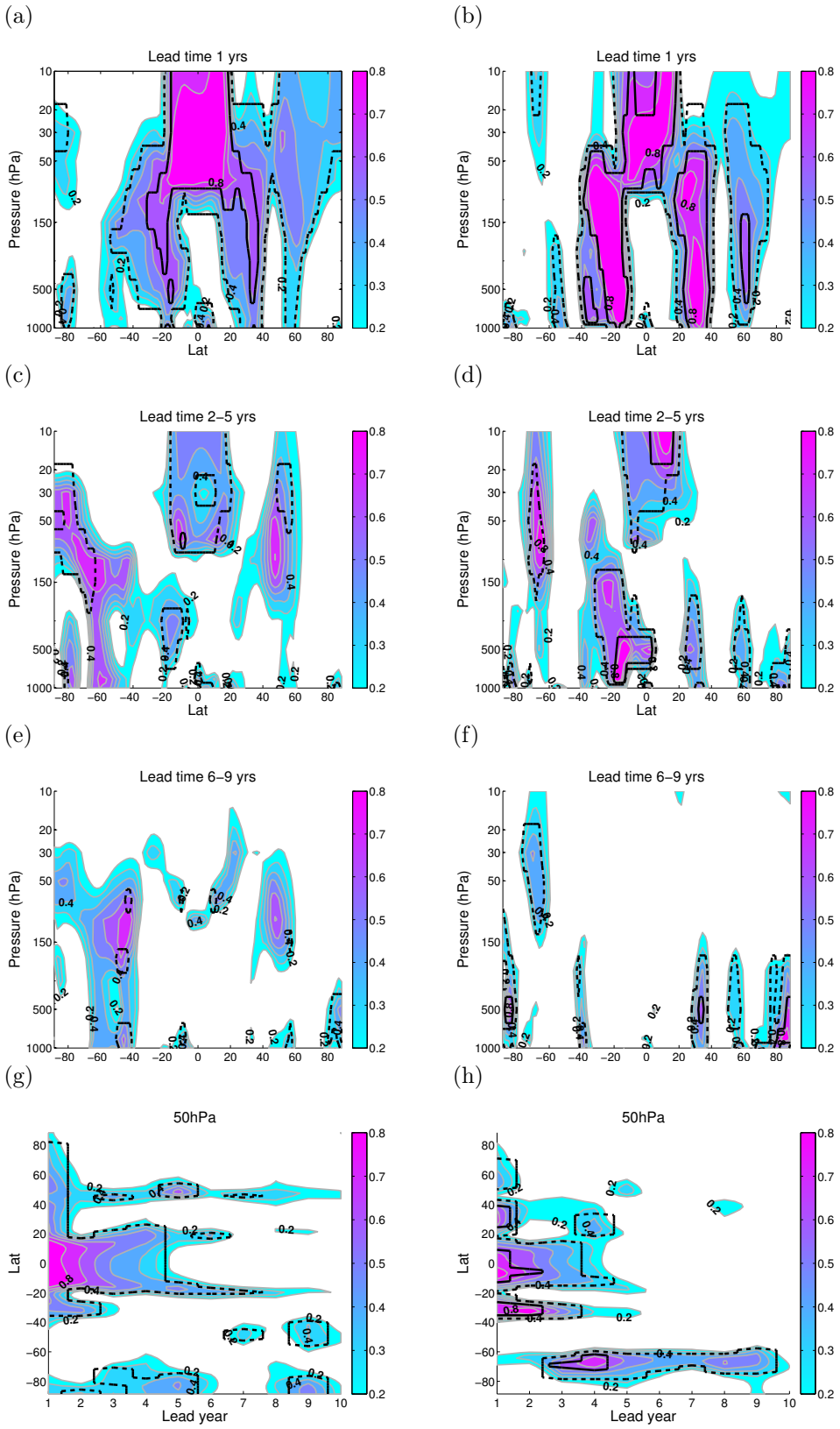

Figure 3.14: ACC of ZMZW hindcasts (left column), differences of initialized minus uninitialized hindcasts (right column); at lead time 1 (a, b); at lead time 2-5 (c,d); at lead time 6-9 (e,f); cross section latitude-lead-year at 50hPa (g,h). Correlation larger than 0.6 are significant at 95% level (solid black line), those larger significant than 0.4 are at 80% level (dashed black line), for MPI-ESM-MR every year initialized.

From yearly initialized hindcasts we select the lead-year 1 that have the zonal mean zonal wind in easterly phase and lead year 1 of westerly wind, based on the QBO index. The QBO index is defined at 50hPa in JFM for equatorial ZMZW greater (lower) than 5 m\s (-5 m\s), see section 4.2 for more details. Figure 3.15 displays the ACC obtained by selecting either the easterly phase (11 years in total) or the westerly phase (13 years in total) of the QBO at lead time 1. The emerging picture suggests that, given the similarity between the patterns in Figure 3.15a and Figure 3.13a (see the 0.8 value of ACC) the easterly QBO phase is sampled more frequently in 5-year hindcasts. In Figure 3.15b is visible also the higher skill in extra-tropical stratosphere in westerly year initialization compared with easterly initialization. This is in agreement with numerous studies that found that the vortex is stronger when equatorial lower stratospheric winds are westerly than when they are easterly (Holton and Tan, 1980, 1982; Labitzke, 1982; Baldwin and Dunkerton, 1991; Dunkerton and Baldwin, 1991). A very interesting result is that Fig. 3.15 indicates more predictive skill from the QBO phase in the SH polar stratosphere than in the NH compared with 3.13a and 3.14a.

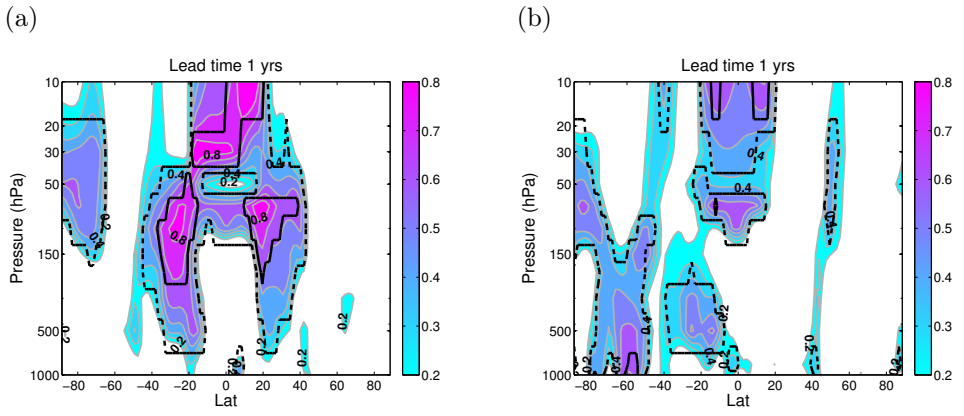

Figure 3.15: ACC of ZMZW at lead-time 1 of easterly years initialized hindcasts (a); westerly years initialized hindcasts (b). Correlation larger than 0.6 are significant at 95% level (solid black line), those larger significant than 0.4 are at 80% level (dashed black line), for MPI-ESM-MR.

Additional information about the high correlation exhibited at lead time 1-5 in Figures 3.13g,h and 3.14g,h at 50hPa-50N, may be given by altitude-lead-time ACC in Figure 3.16. Selected 50N of latitude, we analyse the skill of the hindcasts at different levels at each lead time. The ACC are computed for CMCC-CMS (Fig. 3.16a) and MPI-ESM-MR (Fig. 3.16c,e) runs. What is surprising is the similar patterns of the skill for CMCC-CMS and MPI-ESM-MR (5-yearly and yearly initialized) in Figure 3.16a,c,e. In 5 yearly initialized runs the skill reach 0.8 value at lead time 1 and 5 at 50hPa. With lower skill (0.4) and significant at 80% the yearly initialized hindcasts ACC shows similar result. Future works will be leaded to a better understanding of the high skill existing at 5^{th} lead-time of the ACC at 50hPa-50N, may be related to the ocean initialization.

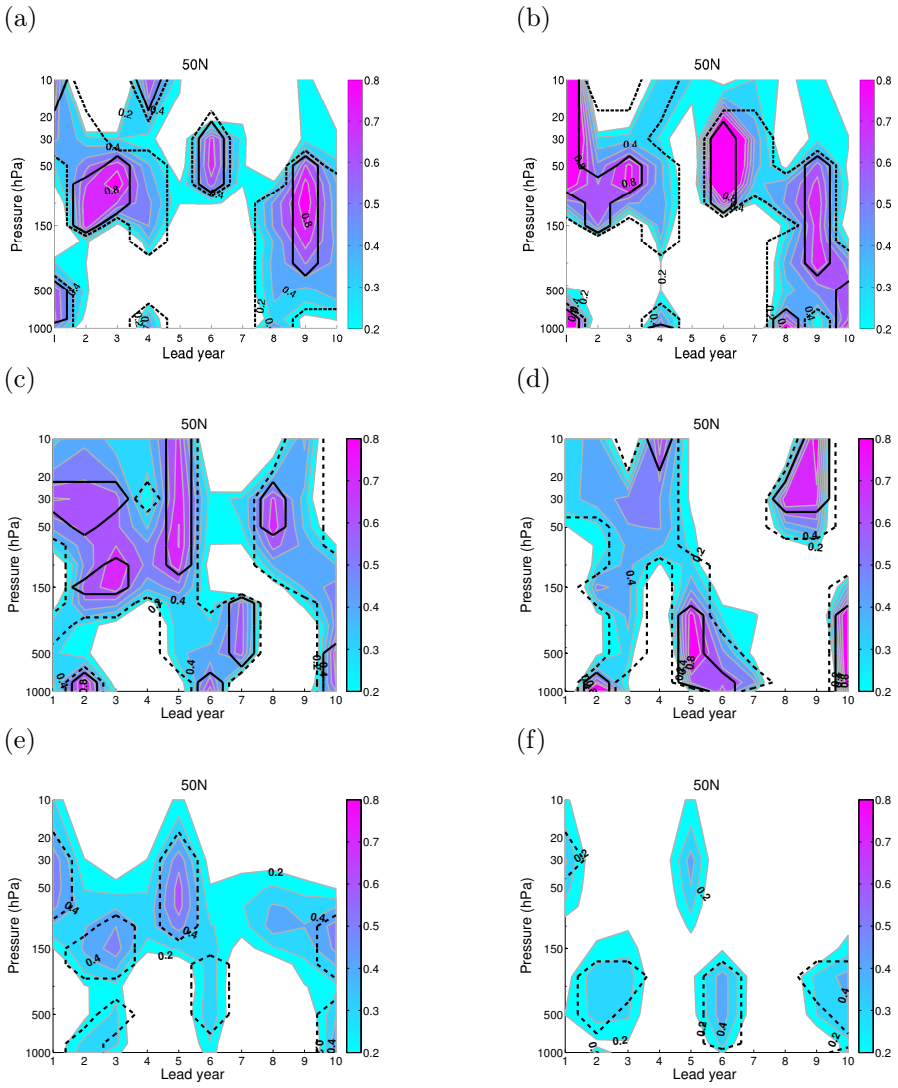

Figure 3.16: ACC of ZMZW cross section altitude-lead-year at 50N hindcasts (left column), differences of initialized minus uninitialized hincasts (right column); CMCC-CMS model (a, b); MPI-ESM-MR 5 year initialized (c,d); MPI-ESM-MR 1 year initialized(e,f).Correlation larger than 0.6 are significant at 95% level (solid black line), those larger significant than 0.4 are at 80% level (dashed black line), for MPI-ESM-MR every year.

In conclusion the ZMZW ACC of the initialized hindcasts for the CMCC-CMS model, increases with lead-time showing patterns of predictive skill attributable to the initial and prescribed boundary conditions of a ocean initialized system. Whereas the ACC regarding the MPI-ESM-MR hindcasts a decrease with lead-time is found, drove by the effect of atmosphere initialization. In agreement with (Pohlmann et al., 2013) and (Scaife et al., 2014) we found with MPI-ESM-MR hindcasts high skill at lead year from 1 to

4 in equatorial stratospheric area, where the variability is dominated by QBO mode. As at NH extra-tropical stratosphere (50hPa) a significant correlation is also found, a connection between the QBO and the polar vortex skill is analysed, following the Holthontan relationship definition (Holton and Tan, 1980).
After an initial thought about a possible aliasing problem, we verified if the loss of significance of 1-year initialization is due to the QBO phase initialization. We conclude that the QBO phase affects the correlations and drives the skill over NH polar vortex zone. Last discussion is leaded in order to find an explanation of the high skill at 5^{th} lead time at 50N-50hPa, however it needs further investigation.

Chapter 4

Sources of predictability, stratospheric dynamics

Significant interannual stratospheric variability in the high latitudes of northern hemispheric zonal wind (Labitzke, 1982; Kodera and Chiba, 1995), is found and attributed to internal atmospheric variability. Part of the variability may be linked to the sudden stratospheric warmings (SSWs) in the extra-tropics (Butchart et al., 2000) and to the quasi-biennial oscillation in the equatorial stratosphere which appears to affect the zonal mean circulation (Holton and Tan, 1982; Dunkerton and Baldwin, 1991; Tung and Yang, 1994). In the next sections we examine the SSWs variability (section 4.1) and a potential QBO influence on extra-tropical predictive skill (section 4.2).

4.1 Sudden stratospheric warming

In this section we examine the statistical proprieties of SSW in both initialized and uninitialized simulations performed with the CMCC-CMS and MPI-EM-MR systems. Particularly through this comparison we intend to highlight the impact of initialization of the ocean (CMCC-CMS) and ocean and atmosphere (MPI-ESM-MR) in SSW variability and predictability.
As polar vortex events, the SSWs are prolonged time periods with an unusually weak and warm northern polar vortex in the winter time. In this study the winter period includes months from November to March (NDJFM). Figure 4.1 shows the daily evolution (from July to June climatological calculated for each calendar day) zonal mean zonal wind (black curve, top panel) at 60N and at 10hPa from ERA40 reanalysis. The bottom panel shows the daily zonal mean of the temperature (black line) at 80N and 10hPa. The dark gray envelopes for both panels indicates the standard deviation and the light gray envelopes are individual maxima and minima from all daily time series (43 years).

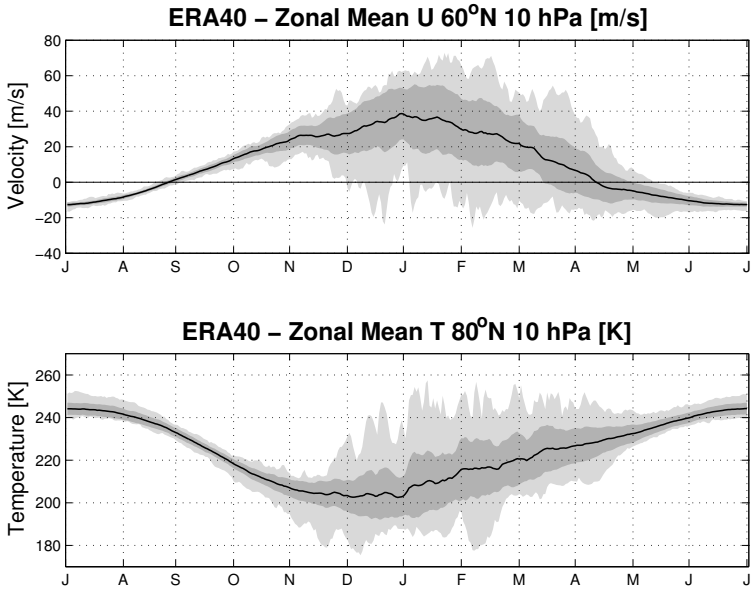

Figure 4.1: Daily zonal mean zonal wind (m/s) at 60N and 10hPa (top) and daily zonal mean temperature (K) at 80N and 10hPa (bottom) for ERA40 reanalysis (1958-2001). Black curves mark climatological averages. Dark gray shading marks the ±1 standard deviation range. Light gray shading marks the daily maxima and minima range.

The zonal mean zonal wind at 60N and 10hPa is westerly during winter and when it reverses to easterly a major midwinter warming is triggered (Fig. 4.1). As Fig. 4.1 shows in light gray, during winter time the daily minima of zonal mean zonal wind at 60N-10hPa (top) coincide with daily maxima of the zonal mean temperature at 80N-10hPa (bottom) for ERA40 daily dataset. Based on this reversal of the zonal mean zonal wind an index is calculated to define SSW event.

4.1.1 SSW detection method

Following the World Meteorological Organization definition (WMO) (Andrews et al., 1985) with Charlton and Polvani (2007b) constrains, the algorithm used in this study is based on an algorithm that only differs from Charlton and Polvani (2007b) study in the definition of the recovery time of the polar vortex after a SSW event. Here, instead of the 20 days established by Charlton-Polvani (see Charlton and Polvani, 2007a, Corrigendum) to define a new event, a time interval greater than 10 days of westerly wind at 10hPa 60N is presumed to be needed after a SSW event. In ERA-40 dataset, for example, this difference has no impact on the number of SSW events. Taking into account this recovery time, placed at 60N-10hPa, the SSW event is found when the zonal wind from westerly becomes easterly in NDJFM.
The algorithm is applied to the daily zonal mean zonal wind at 10 hPa of initialized (1^{st} of January) and uninitialized simulations for CMCC-CMS and MPI-ESM-MR models.

The SSW events are identified for each start date over all 10 year hindcasts for each ensemble member (3x100 years in all). The uninitialized simulations are divided into 10 years chunks in order to obtain a twin set comparable to the decadal hindcasts. In order to have a longer period of observed SSW events here we extend the ERA-40 time series reanalysis with ERA-Interim reanalysis holding years from 1961 to 2010.

4.1.2 Distribution of SSW events

The influence of ocean initialization on the SSW statistics is investigated with the CMCC-CMS model, using the methodology outlined in section 4.1.1.
The winter (NDJFM) frequency of occurrence of SSW events is computed for both initialized and uninitialized runs. In Figure 4.2a each yellow bar represents the ensemble averaged SSWs frequency computed for each 10 years hindcasts over the full period from 1961 to 2015. In Figure 4.2b SSWs are diagnosed for the uninitialized run. Here 10-year chunks are taken so as to correspond to the decadal hindcasts, over the period from 1961 to 2005. The mean computed across all start dates is also shown in black line.
From the analyses in Figure 4.2a the distribution of the SSW shows a pronounced intraseasonal variability with maximum of occurrence around February-March. The observed SSW frequency in Figure 4.2c (black bars) features an intraseasonal variability of similar amplitude, but with a maximum around January-February.
As a general tendency it appears that, compared to observational estimates, SSWs are overestimated in initialized hindcasts and underestimated in the uninitialized simulation. Thus the influence of ocean initialization seems to act on the variability of SSWs, with the hindcasts systematically overcoming the frequency of occurrence of SSW featured by the uninitialized simulation. In the specific the initialization changes the seasonality of the SSWs, shifting the maximum of occurrence in March.
The high decadal variability of SSWs, found also in the initialized hindcasts, suggests the empirical nature of the SSWs classification. As the identification of SSWs is sensitive to definition, different diagnostics could be also checked. There is a current effort to develop consensus on updating the SSW definition (Butler et al., 2014, submitted).

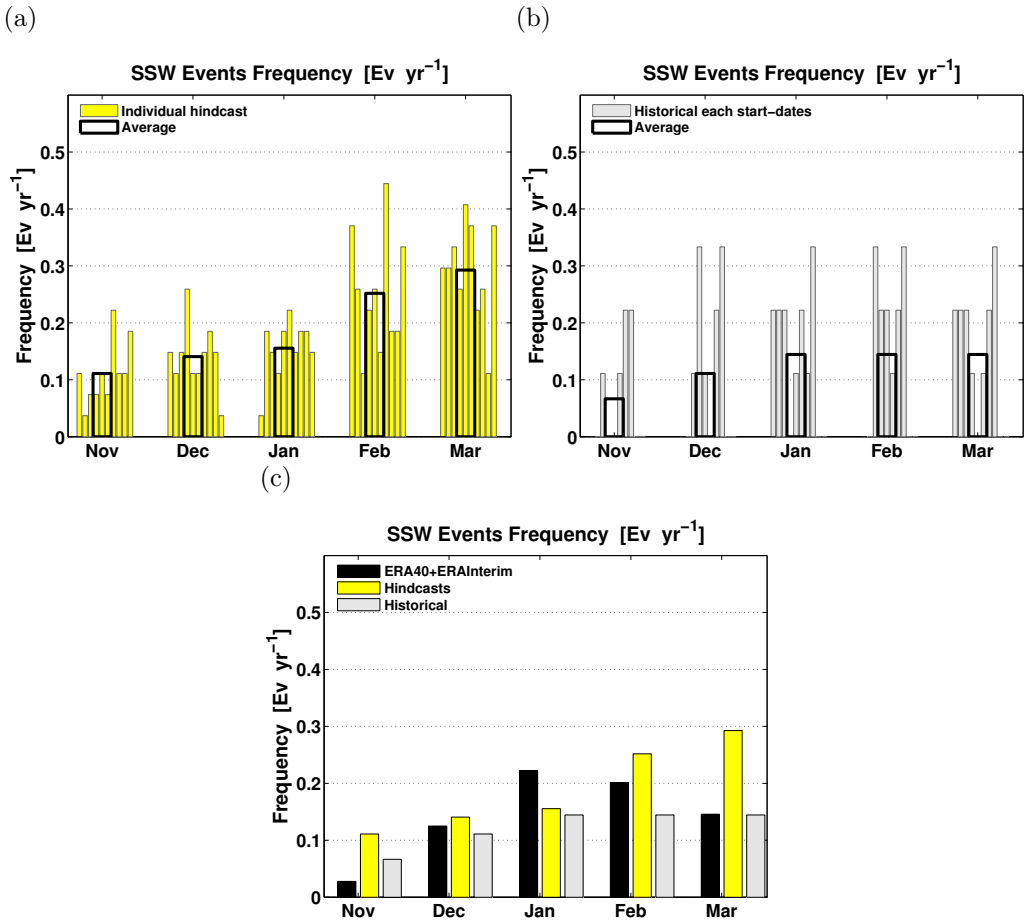

Figure 4.2: Frequency of occurrence of sudden stratospheric warmings a) ensemble averaged for 10 years at each start date (yellow bars); b) for 10 years chunked at same start date; the mean across all start date is in black line; c) mean across all strat date for hindcasts (yellow bars) and for historical (gray bars) together with ERA-40-ERA-Interim reanalysis (black bars) distribution, after Charlton and Polvani, 2007. The simulations are from CMCC-CMS model.

Next, the combined effect of ocean and atmosphere initialization is inspected through the analysis of MPI-ESM-MR hindcasts and historical simulations. To allow a fair comparison with CMCC-CMS decadal prediction experiments, we first inspect the MPI-ESM-MR simulations by considering a 5-yearly sub-sample of the full MPI-ESM-MR experimental set.

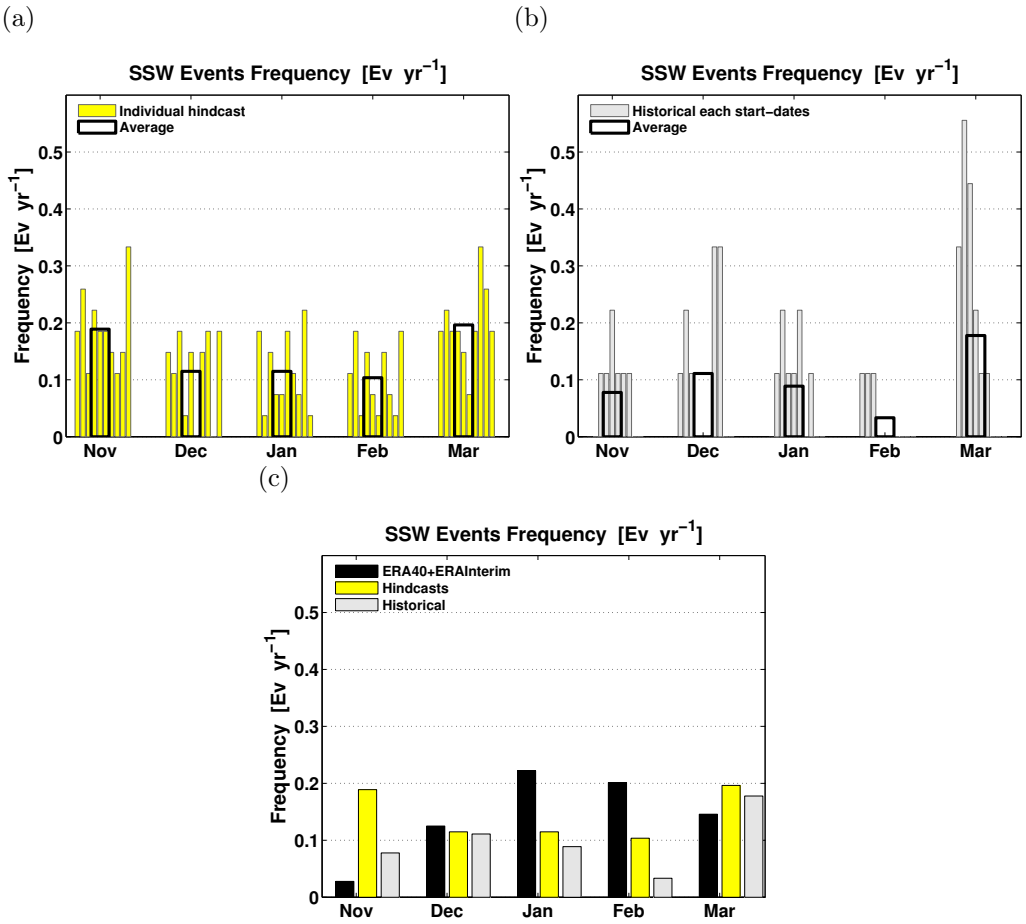

Figure 4.3: Frequency of occurrence of sudden stratospheric warmings a) ensemble averaged for 10 years at each start date (yellow bars); b)ensemble averaged for 10 years chunked at same start date; the mean across all start date is in black line; c) mean across all strat date for hindcasts (yellow bars) and for historical (gray bars) together with ERA-40-ERA-Interim reanalysis (black bars) distribution after Charlton and Polvani, 2007. The simulations are from MPI-ESM-MR 5-yearly initialized model.

As in Figure 4.2, Figure 4.3 shows the NDJF distribution of occurrence of SSW with the only difference that the SSWs frequency are ensemble averaged also for the historical runs. Similarly to CMCC-CMS the observed intraseasonal variability is not well reproduced by MPI-ESM-MR hindcasts. These feature relative maxima in November and March (instead of January, as shown in the reanalysis). Also, hindcasts feature a SSW frequency which is systematically higher than in the historical runs, consistent with the results found for CMCC-CMS.
In the previous analysis the full 10-year length of the hindcasts (and uninitialized runs slices) was exploited. Next we want to have a closer look at the effect of initialization by considering individual lead-times.

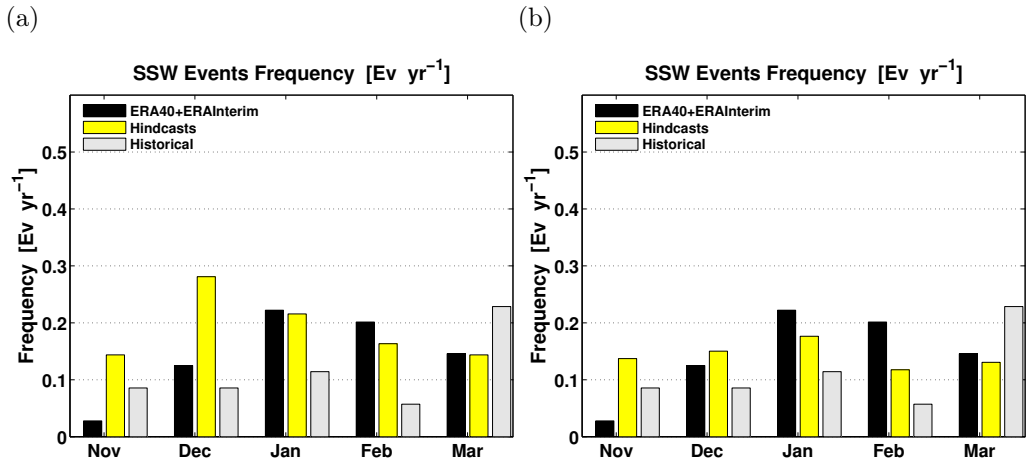

Figure 4.4: Frequency of occurrence of sudden stratospheric warmings ensemble averaged for a) lead time 1; b) lead time 5; for hindcasts (yellow bars) and for historical (gray bars) together with ERA-40-ERA-Interim reanalysis (black bars) distribution after Charlton and Polvani, 2007. The simulations are from MPI-ESM-MR yearly initialized model.

As the hindcasts are initialized in January, the atmosphere initialization may have a greatest influence in the SSW frequency in January and in the successive months.
For this reason and to avoid the overlapping between hindcast years corresponding to consecutive start dates, the atmosphere initialization effects are investigated over the lead year 1 of the yearly initialized simulation of the MPI-ESM-MR model.
In Figure 4.4a the yellow bars represent the SSW frequency computed considering only lead year 1 from each yearly hindcasts. Interestingly once we consider only lead year 1, the observed intraseasonal winter variability of SSWs is better reproduced compared with previous cases.
We also investigate the distribution of SSWs for all other lead times (not shown). Between all, the best fit of to the intraseasonal distribution is found at 5^{th} lead time (Fig. 4.4b) which displays a qualitative agreement with the observed SSWs. This is in agreement with the higher skill of the ZMZW found in the polar vortex region (50N-50hPa) at 5^{th} lead time in section 3.3.2. The result from the monthly distribution at lead time 5 of the SSWs, which are related to the changes of the polar vortex, may be attributed to the ocean initialization effects. The ocean initialization might have the potential to affect the atmosphere on multi-year time scales, given his inherently longer memory, as compared to the atmosphere.
Afterwards we examine the inter-annual variability of SSW in the reanalysis together with hindcasts and historical simulations for CMCC-CMS and MPI-ESM-MR runs, the latter for both yearly and 5-yearly initialization.
From Fig. 4.5 to Fig. 4.7 the number of SSWs are displayed in 5-year bins. The 5 years bin are chosen so as to avoid the overlapping between consecutively 10 years chunks, when counting the SSWs, following Charlton and Polvani (2007b). Bins are selected in the following way: 1963-1967 in 1965 bin, 1968-1972 in 1970 bin , 1973-1977 in 1975 bin,

and so forth. In this case the yellow scale color bars describe the number of SSWs for each ensemble members. The number of SSWs is then ensemble averaged, and is shown in black line.

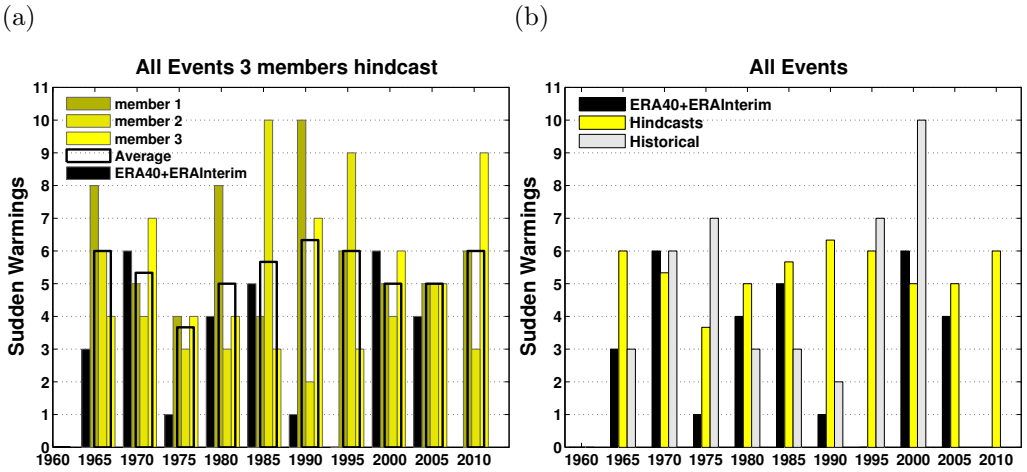

Figure 4.5: Distribution of sudden stratospheric warmings. Diagnostic shows number of SSWs in 5-yr bins a) in each ensemble member (yellow scale color bars) of the hincasts with ensemble averaged number of SSWs in black line; b) ensemble averaged number of SSWs for hindcasts (yallow bars), number of SSWs in the historical run (gray bars). In black bars are SSWs number in ERA-40-ERA-Interim reanalysis in both panels. The simulations are from CMCC-CMS model.

In Figures 4.5a each ensemble member displays a strong inter-annual variability in the CMCC-CMS. After averaging the SSWs number over the ensemble members (yellow bar in Fig. 4.5b), the SSW variability in the decadal integrations is grossly consistent with the observations (black bars). However, the amplitude of the inter-annual fluctuations in the initialized hindcasts SSWs is weaker than in the observed, mainly due to the lack of zero-event periods in the model record. The inter-annual fluctuation of the SSWs in the historical run shown in Figure 4.5b (gray bars) exhibit a higher inter-annual variability compared with the initialized hindcasts. Maybe this higher variability is related to the fact that the historical run has a single ensemble member.
The same analyses is applied for MPI-ESM-MR model, for 5-yearly sub-sampled initialized simulations. The number of SSWs to the the individual ensemble members (yellow scaled color bars, Fig. 4.6a) exhibits less spreading compared with CMCC-CMS distribution. The SSWs appear with a higher variability in the historical ensemble members in respect to initialized hindcasts.

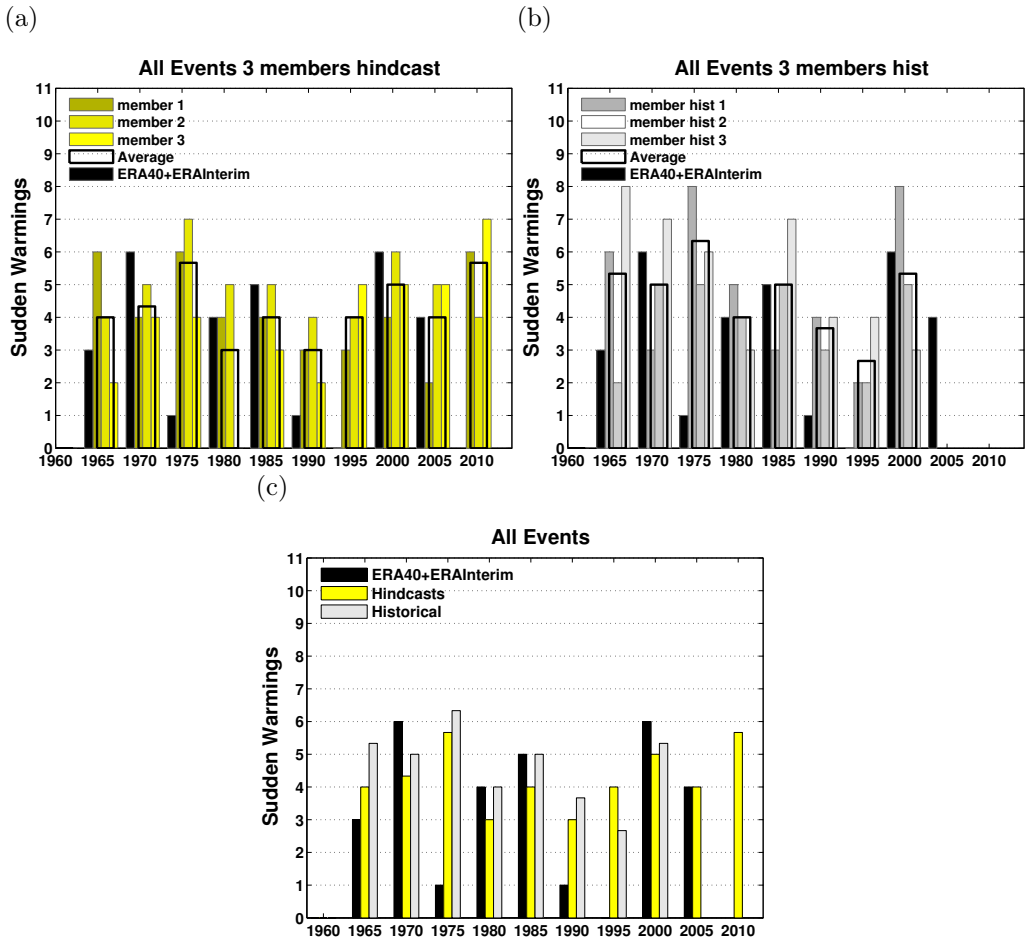

Figure 4.6: Distribution of sudden stratospheric warmings. Diagnostic shows number of SSWs in 5-yr bins a) in each ensemble member (yellow scale color bars) of the hincasts; b) of the historical, with ensemble averaged number of SSWs in black line; c) ensemble averaged number of SSWs for hindcasts (yallow bars), for the historical runs (gray bars). In black bars are SSWs number in ERA-40-ERA-Interim reanalysis in all panels. The simulations are from MPI-ESM-MR 5-yearly initialized model.

Figure 4.6c shows the ensemble averaged SSWs distribution of initialized and uninitialized simulations, both having a similar variability but still not caching the minima and the zero observed in 1995 (black bars).
The diagnostic is applied also to the MPI-ESM-MR yearly initialized hindcasts. Figure 4.7a shows the SSWs number for each ensemble member at lead time 1. In this case the period includes 1961-2011 corresponding to each start date. The uninitialized simulations cover a period from 1961 to 1995 4.7b.
Number of SSWs is largely different from member to member (Fig. 4.7a) and from the ensemble averaged distribution the inter-annual variability of SSWs (Fig. 4.7c) seems to follow the observed variability. We examined also the SSws distribution at lead time 5

(1965-2015), that is qualitatively concordant with the reanalysis (Fig. 4.7d).
In both cases lead time 1 and 5 the lack of the SSWs is missed.

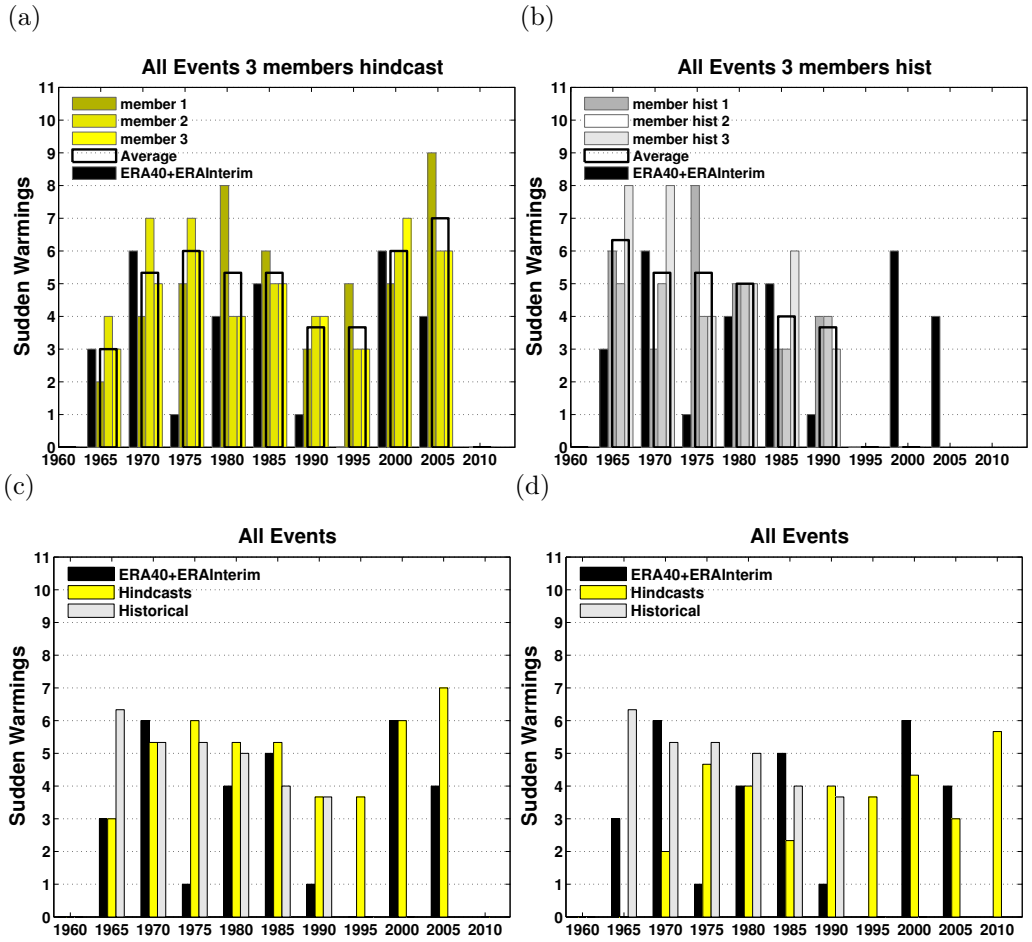

Figure 4.7: Distribution of sudden stratospheric warmings. Diagnostic shows number of SSWs in 5-yr bins a) in each ensemble member (yellow scale color bars) of the lead time 1 (1961-2005); b) of the historical (1961-1995), with ensemble averaged number of SSWs in black line; c) ensemble averaged number of SSWs for lead time 1 (yallow bars), for the historical runs (gray bars). In black bars are SSWs number in ERA-40-ERA-Interim reanalysis in all panels. d) as c) for lead time 5 (1965-2010). The simulations are from MPI-ESM-MR yearly initialized model.

Summarising and concluding, in this section the intraseasonal and interannual variability of the sudden stratospheric warmings for CMCC-CMS and MPI-ESM-MR models are examined. The study is based on the comparison between the initialized with uninitialized SSW event distribution.
We may conclude that in general both variability and predictability of SSWs are sensitive

to the initialization.
The intraseasonal variability (NDJFM) is not correctly represented for 5 yearly initialization (CMCC-CMS, MPI-ESM-MR), but it considerably improve for yearly initialization. Some degree of predictability is also found under conditions sufficiently high of sampling at lead time 1 and 5. While the SSW events frequency at lead time 1 may be affected by atmosphere initialization, at lead time 5 the SSWs occurrence may be influenced by the initialization of the ocean, due to time scales typically longer than those of atmosphere-only processes.
At inter-annual time scale as general and common results we found that the hindcasts are only qualitatively consistent with the observed year-to-year SSW variability. However, model results appear to be unable to reproduce "zero-events" periods, as detected in observational records.

4.2 Holton-Tan relationship

The aim of this section is to analyse the interannual predictability of the zonal wind in the northern hemispheric stratosphere and investigate a potential QBO influence on extra-tropical predictive skill.
The effect of the QBO on stratospheric vortex may be seen by comparing composites of extra-tropical zonal-mean wind during easterly and westerly phases of the QBO. The QBO phase must be defined precisely, and typically the equatorial zonal-mean wind at a particular level is used. Holton and Tan (1980) defined the QBO phase using equatorial winds at the 50 hPa level, but other authors have used also different levels.

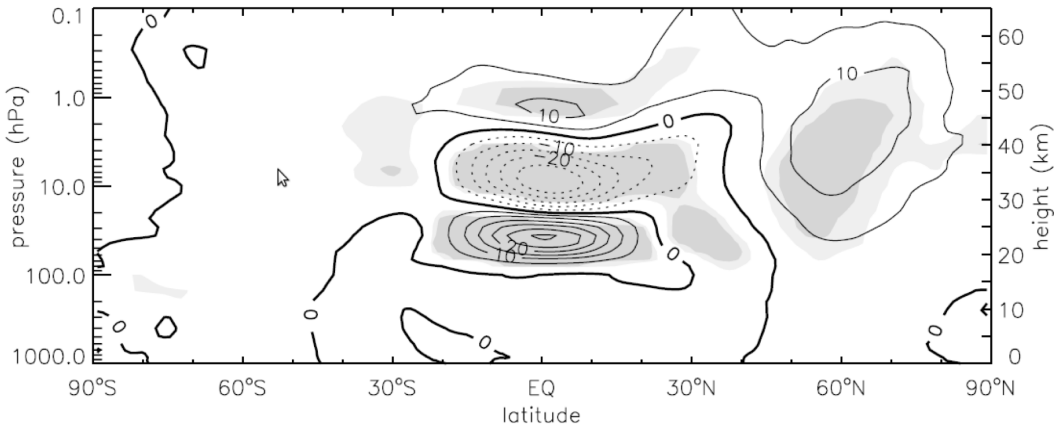

Figure 4.8: December-January zonal mean zonal wind difference for QBO westerly minus QBO easterly years at 44hPa with t-test confidence shading shown at 95% and 99%; contours are at 5 m/s intervals; ERA-40 data for the period period January 1958 to December 2001. From Pascoe et al. (2005)

In Figure 4.8 for example the composite for the zonal- mean zonal wind anomalies for

DJ based on an index defined as the ZMZW at 44 hPa, using ERA40 reanalysis (Pascoe et al., 2005). In this figure, the westerly minus easterly difference shows an unequal dipole with very small zonal mean zonal wind differences south of 45 S. The NH zero correlation wind line is also clearly visible. The plot displays a tripolar vertical phase structure of the QBO zonal wind anomalies. The difference of westerly minus easterly is positive in the upper stratosphere from 1 to 0.1 hPa, negative in the middle from 10 to 1 hPa and then positive in the lower stratosphere below 10 hPa (Gray et al., 2004; Pascoe et al., 2005). The tripolar phase structure is a signature of downward propagation of the QBO signal generated by the descent of a QBO phase followed by a new phase present in the upper stratosphere and anticipated by an earlier phase in the lower stratosphere of the opposite sign. The zonal wind anomalies extend to the subtropics in the Northern Hemisphere up to about 50 N and are dominated by a modulation of the polar vortex which extends from the surface to the 1 hPa level (Baldwin et al., 2001).
Here we computed a QBO index (see section 4.2.1) following the Holton and Tan (1980) definition, applied to the ERA40 reanalysis, initialized and uninitialized simulations.

4.2.1 Quasi-biennial oscillation Index

Based on Holton and Tan (1980) the QBO index is calculated as below. Westerly (easterly) wind is defined when the ZMZW in January-February-March at 50hPa in the equator region (10S-10N) is larger (smaller) than 5 m\s (-5 m\s) as wind threshold. Based on this index westerly (easterly) years were selected. The composites are calculated by subtracting easterly years from westerly years. In the ERA40 reanalysis from 1961-2002 the composite counts 15 westerly years and 10 easterly years. Equivalently to the observed, when we applied the QBO index the lead-time 1 of the MPI-ESM-MR hindcasts we found 14 westerly years and 11 easterly years for yearly initialized runs from 1961 to 2012, and 4(3) westerly(easterly) years for 5-yearly initialized sub-sampled runs. In the historical runs (both model) and CMCC-CMS hindcasts, the QBO phase is not in phase with the observed one, as no initialization in the atmosphere is used.

4.2.2 Composites

Figure 4.9b shows the composites of zonal-mean zonal wind for MPI-ESM-MR yearly initialized in JFM and compared with composites of reanalysis (Fig. 4.9a) the HTR appears to be well described by the initialized simulations. The alternate westerly and easterly winds are found in the equatorial atmosphere, with a clear presence of the QBO in the equatorial stratosphere in the hindcasts, in agreement with the atmosphere initialization. The anomalies clearly show the vertically propagating signal in the extratropical regions, validating the HTR in the model. Maximum values are about 20 m/s in equatorial regions and about 8-10 m/s in polar vortex area, spanning from about 150 hPa to above 10 hPa.

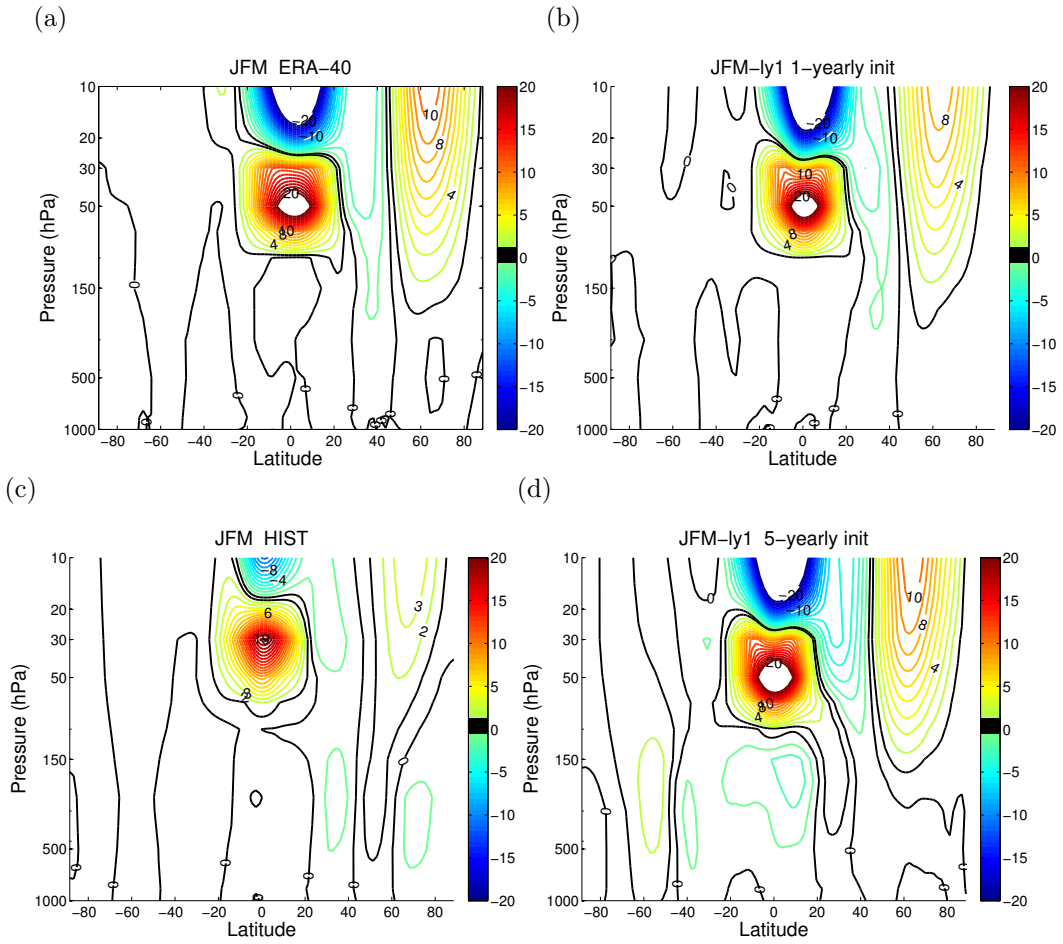

Figure 4.9: Composites of the zonal mean zonal wind anomalies (m/s) based on the QBO winter (JFM) index (see text for details) from (a) ERA-40 reanalysis and from MPI-ESM-MR (b)1-yearly initialized hindcasts; (c) historical and (d) 5-yearly initialized simulations. Only lead-year 1 is considered in the hindcasts.

Further analysis are made by considering the historical run in order to see the impact of the ocean-atmosphere initialization on the HTR. The HTR is weaker in the uninitialized runs (Fig. 4.9c) with respect to the initialized and reanalysis. This validates the importance of the atmosphere initialization for a better predictability of the ZMZW. Additionally in agreement with Schirber et al. (2014) larger values of easterly winds reach lower altitudes in the lower stratosphere in ERA and initialized runs compared to unitilized runs, but ends at 50 hPa rather that 90 hPa. The different behaviour of the HTR may also be related to ENSO. ENSO is one of the largest models of variability in the climate system, and results of numerous studies have established a strong influence of ENSO on the vortex (e.g. Wallace and Chang 1982; Free and Seidel 2009). To summarize, the mean vortex temperature is greater during WENSO (warm ENSO phase) than CENSO (cold ENSO phase) by about the same difference between QBO-E and QBO-W

winters. The zonal mean zonal wind has been found to be smaller and displace south during WENSO in January and February (Mitchell et al., 2011) with CENSO living rise to opposite and smaller anomalies. On average, ENSO influence appears later in the winter stratosphere than the QBO. Butler and Polvani (2011) also found that SSWs are more frequent during both large WENSO and CENSO events than during neutral ENSO years, however those results do not have a large statistical significance. A large numbers of modeling studies have shown that warmed and weakened vortex during WENSO events are due to enhanced wavenumber-1 planetary wave forcing in the stratosphere (e.g. Manzini et al. 2006; Cagnazzo and Manzini 2009; Sassi et al. 2004; Ineson and Scaife 2009). Moreover, there is observational and modeling evidence that QBO and ENSO influence the vortex through a non-linear interaction (Garfinkel and Hartmann (2007); Calvo et al. (2009). These results indicate that if in the historical uninitialized QBO composites, the number of WENSO and CENSO years included is different than in the initialized runs, this could lead to differences in the HTR due to the ENSO-QBO interaction. This possible result is not verified here, but will be analysed in a next study. The composites are calculated also over the sub-sampled 5-yearly initialized runs (Fig. 4.9d) that show stronger jets in equatorial stratosphere and the related signal in polar vortex domain, compared to yearly initialized hindcasts. This is in agreement with the result found in section 3.2.2 according to which in 5-yearly initialized hindcasts the skill shows higher significance related to the QBO phase in respect to the yearly initialized runs, in these two regions.
For a better understanding of the initialization influence in the HTR representation we diagnose the ZMZW composites from the CMCC-CMS simulations (Fig. 4.10a).

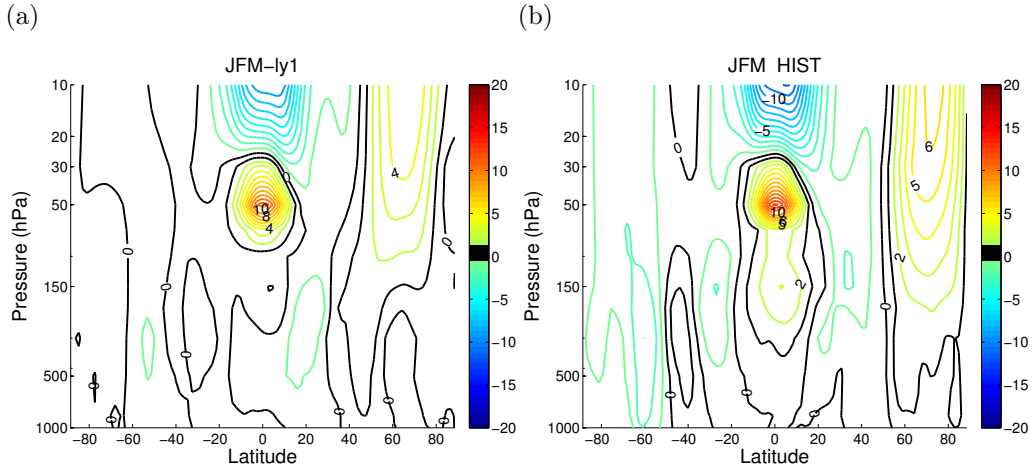

Figure 4.10: Composites of the zonal mean zonal wind anomalies (m/s) based on the QBO winter (JFM) index (see text for details) from CMCC-CMS (a) 1-yearly initialized hindcasts; (b) historical. Only lead-year 1 is considered in the hindcasts.

Compared to reanalysis and MPI-ESM-MR results, it is clearly shown a weaker alternation of westerly-easterly (maximum is 10 m/s) structure and less intense polar vortex

signal. This finding makes clear the importance of the atmosphere initialization, leading to enhanced skill in the equatorial stratospheric region together with a better simulated HTR in the near term predictions. Extra investigation about initialization effect on HTR is made through the composite of CMCC-CMS historical ZMZW (Fig. 4.10b). From a comparison between the composite for the initialized hindcasts and the composite for historical run similar structure and intensity values are found. This suggests that the HTR in the simulations is not affected by the ocean initialization. The QBO has effects on the strength of the polar vortex, this connection is found in the initialized hincasts through a QBO index calculated considering JFM of lead time 1, computing the composites as west minus east QBO phase. The result of a well-reproduced HTR by initialized hindcasts of MPI-ESM-MR confirms the importance of the initialization of the atmosphere, providing evidence that a proper initialization of the QBO might be beneficial not only for the predictability of the extra-tropics.

Chapter 5

Discussion and conclusions

In this work, the role of the stratosphere on the multi-annual predictability of the climate system has been examined. This topic has been approached with the innovative experimental framework of decadal predictions, recently adopted in the CMIP5 effort, as part of the IPCC AR5 assessment. Specifically, two sets of decadal hindcasts performed with state-of-the-art climate models, including a well-resolved stratosphere (CMCC-CMS and MPI-ESM-MR) were analysed in order to evaluate the separate impact of a realistic ocean and atmosphere initialization.
A first look was dressed to the surface temperature skill, assessing that both ocean and atmosphere initializations give globally an improvement to the predictive skill. Succeeding the attention was leaded to the atmospheric variable zonal wind averaged zonally. As result the skill associated with the zonal wind for ocean initialized system (CMCC-CMS) increases with lead-time, attributable to the initial and boundary conditions influence. While the effect of the atmosphere initialization on the (MPI-ESM-MR) hindcasts decreases with lead-time, consistently with the memory time scale of the atmosphere initialization effects. An important aspect of the initialization effect is given by considering the initialization at different QBO phases. It suggests a dependency of the skill from the QBO phase initialization.
After the predictive skill verification, this study moved to the investigation of the ocean/ atmosphere initialization impact on the variability and predictability of two stratospheric mechanisms, such as SSWs events and the QBO-polar vortex connection.
The initialization effects on the SSWs are analysed at both intraseasonal and interannual scales. The study of SSW variability is based on the comparison between the initialized with uninitialized SSW event distribution. In general CMCC-CMS model overestimate the SSWs observed in the initialized simulations. Specifically, results from the MPI-ESM-MR (atmosphere-initialized) model show an improvement on boreal winter (NDJFM) intraseasonal variability. The intraseasonal distribution of events is not in agreement with observations, also if the yearly initialized simulations show a considerably improvements compared with 5 yearly initialized runs. The interannual variability in the initialized hindcasts is qualitatively consistent with the observed year-to-year SSW variability, but the "zero-events" detected in observational records are never reproduced by any of the

inspected models.
The interannual predictability of the zonal wind in the northern hemispheric stratosphere and a potential QBO influence on extra-tropical predictive skill were also investigated. In agreement with (Pohlmann et al., 2013) and (Scaife et al., 2014) we found with yearly initialized MPI-ESM-MR hindcasts significant skill at lead year from 1 up to 4 in equatorial stratospheric area, where the variability is dominated by QBO mode. The influence of atmosphere and ocean initialization, and in particular of the connection between equatorial stratosphere (through the QBO phase) and the extra-tropical circulation (polar vortex strength) has been inspected, through an analysis of the Holton-Tan relationship in the two decadal prediction systems. From analysis of the composites the importance of the initialization of the atmosphere is confirmed by the well reproduced HTR from MPI-ES-MR yearly initialized hindcasts. Interesting information is given by the uninitialized run of CMCC-CMS showing that the ocean initialization has not influence in the HTR representation.
These results suggest that the atmosphere initialization has a key role on the variability and predictability of stratospheric processes providing evidence that a proper initialization of the QBO might be beneficial not only for the predictability of the tropics but also in the extra-tropics. However the ocean initialization gives additional improvement of the skill at longer term prediction. The ocean initialization influence needs to be analysed further as enhanced skill is found at longer term. Subject of investigation can be an ocean-atmosphere connection with multi-decadal oscillation in North Atlantic of the SSTs. This analyses may help to understand processes related to the skill of the zonal wind found in the lower stratosphere.

Bibliography

Ambaum, M. H. P. and Hoskins, B. J. (2002). The nao troposphere-stratosphere connection. *J. Climate,*, 15:1969–1978.

Andrews, D. G., Holton, J. R., and Leovy, C. B. (1985). Middle atmosphere dynamics. *Academic Press*, page 489.

Andrews, D. G., Holton, J. R., and Leovy, C. B. (1987). Middle Atmosphere Dynamics. *Academic Press, San Diego, California,*, page 489.

Angell, J. K. and Korshover, J. (1962). The biennial wind and temperature oscillation of the equatorial stratosphere and their possible extension to higher latitudes. *Mon. Weather Rev.*, 90:1205–1208.

Anstey, J. A., Shepherd, T. G., and Scinocca, J. F. (2010). Influence of the quasi-biennial oscillation on the extratropical winter stratosphere in an atmospheric general circulation model and in reanalysis data. *J. Atmos. Sci.*, 67:1402–1419.

Balachandran, N.K .and Rind, D. (1995). Modeling the effects of UV variability and the QBO on the troposphere-stratosphere system. Part I: the middle atmosphere. *J. Climate*, 8:2058 – 2079.

Baldwin, M. and Dunkerton, T. (1991). Quasi-biennial oscillation above 10 mb. *Geophys. Res. Lett.*, 18:1205–1208.

Baldwin, M. and Dunkerton, T. (2001). Stratospheric harbingers of anomalous weather regimes. *Science*, 294:581–584.

Baldwin, M. P., Stephenson, D. B., . Thompson, D. W. J., Dunkerton, T. J., Charlton, A. J., and O'Neill, A. (2003). SStratospheric memory and extended-range weather forecasts. *Science*, 301(301):636–640.

Baldwin, M. P. et al. (2001). The quasi-biennial oscillation. *Rev. Geophys.*, 39: 179 – 229.

Balmaseda, M. A., Mogensen, K., and Weaver, A. T. (2012). Evaluation of the ecmwf ocean reanalysis system oras4. *Q. J. R. Meteorol. Soc.*, 139:1132–1161.

Barnston, A. G., Glantz, M. H., and He, Y. (1999). Predictive skill of statistical and dynamical climate models in forecasts of SST during the 1997-98 El Niño episode and the 1998 La Niña onset. *Bull.Amer. Meteor. Soc.*, 80:217–244.

Bellucci, A., Gualdi, S., Masina, S., Storto, A., Scoccimarro, E., Cagnazzo, C., and ... & Navarra, A. (2013). Decadal climate predictions with a coupled OAGCM initialized with oceanic reanalyses. *Climate dynamics*, 40(5-6)):1483–1497.

Bellucci, A., Haarsma, R., Gualdi, S., Athanasiadis, P., and Co-Workers (2014). An assessment of a multi-model ensemble of decadal climate predictions. Climate Dynamics. *J. Adv. Model. Earth Syst.*

Boer, G. J. and Hamilton, K. (2008). QBO influence on extratropical predictive skill. *Climate Dynamics.*, 31:7-8:987–1000.

Brohan, P., Kennedy, J., Harris, I., Tett, S., and Jones, P. (2006). Uncertainty estimates in regional and global observed temperature changes: a new dataset from 1850. *J. Geophysical Research*, :111.

Brovkin, V., Boysen, L., Raddatz, T., Gayler, V., Loew, A., and Claussen, M. (2013). Evaluation of vegetation cover and land-surface albedo in MPI-ESM CMIP5 simulations. *J. Adv. Model. Earth Syst*, 5:48–57.

Butchart, N., Austin, J., Knight, J. R., Scaife, A. A., and Gallani, M. L. (2000). The response of the stratospheric climate to projected changes in the concentrations of well-mixed greenhouse gases from 1992 to 2051. *J. Climate*, 13:2142-2159.

Butler, A. and Polvani, L. (2011). El Niño, La Niña, and stratospheric sudden warmings: A reevaluation in light of the observational record. *Geophys. Res. Lett*, 38(13).

Butler, A. H., Seidel, D. J., Hardiman, S. C., Butchart, N., Birner, T., and Match, A. (2014). Defining sudden stratospheric warmings . *Bulletin of the American Meteorological S*, submit:March.

Cagnazzo, C. and Manzini, E. (2009). Impact of the stratosphere on the winter tropospheric teleconnections between ENSO and the North Atlantic and European region. *J. Climate*, 22(5):1223–1238.

Cagnazzo, C., Manzini, E., Giorgetta, M., De F. Forster, P., and Morcrette, J. (2007). Impact of an improved shortwave radiation scheme in the MAECHAM5 General Circulation Model. *Atmos Chem Phys*, 7:2503–2515.

Calvo, N., Giorgetta, c., and Peña-Ortiz, C. (2007). Sensitivity of the boreal winter circulation in the middle atmosphere to the Quasi-Biennial Oscillation in MAECHAM5 simulations. *J.Geophys.Res.*, 112.

Calvo, N., Giorgetta, M., Garcia-Herrera, R., and Manzini, E. (2009). Nonlinearity of the combined warm ENSO and QBO effects on the Northern Hemisphere polar vortex in MAECHAM5 simulations. *Res.J. Geophys.*, 114(D13):32–36.

Camp, C. and Tung, K. (2007). The infuence of the solar cycle and QBO on the late-winter stratospheric polar vortex. *J. Atmos. Sci.*, 64):1267–1283.

Charlton and O'Neill, A. (2003). Stratospheric memory and skill of extended-range weather forecasts. *Science*, 301:636–640.

Charlton, A. J. and Polvani, L. M. (2007a). Corrigendum. `http://www.columbia.edu/~lmp/paps/charlton+polvani-JCLIM-2007-CORRIGENDUM.pdf`.

Charlton, A. J. and Polvani, L. M. (2007b). A new look at stratospheric sudden warmings. part i: Climatology and modeling benchmarks. *J. Climate*, 20:449.

Charlton, A. J. et al (2007). A new look at stratospheric sudden warmings. part ii: Evaluation of numerical model simulations. *J. Climate*, 20:470.

Charney, J. G. and . Drazin, P. G. (1961). Propagation of planetary scale disturbances from the lower into the upper atmosphere. *J.Geophys. Res.*, 66:83–109.

Christiansen, B. (2005). Downward propagation and statistical forecast of the near-surface weather. *J. Geophys. Res.*, 110:D14104.

CMIP-WGCM-WGSIP, D. C. P. P. (2011). Data and bias correction for decadal climate predictions. *Geophys. Res. WCRP Rep., ICPO Publ.*, 150:3.

Cohen, J., Barlow, M., Kushner, P. J., and Saito, K. (2007). Stratosphere-troposphere coupling and links with Eurasian land surface variability. *J.Climate*, 20:5335–534.

Dee, D. P. and co authors, . (2011). The ERA-Interim reanalysis: Configuration and performance of the data assimilation system. *T. Quart. J. R. Meteorol. Soc.*, 137:553–597.

Du, H., Doblas-Reyes, F. J., GarciÌĄa-Serrano, J., GueÌĄmas, V., and Soufflet, Y. and-Wouters, B. (2012). Sensitivity of decadal predictions to the initial atmospheric and oceanic perturbations. *Climate Dyn*, 39:2013–2023.

Dunkerton, T. and Baldwin, M. (1991). Quasi-biennial modulation of planetary-wave fluxes in the Northern Hemisphere winter. *J. Geophys. Res.*, 100(D6):11055–11068.

Dunkerton, T. J. and Delisi, D. P. (1985). Climatology of the equatorial lower stratosphere. *J. Atmos. Sci.*, 46:3343–3382.

Fichefet, T. and Morales-Maqueda, M. A. (1999). Modeling the influence of snow accumulation and snow-ice formation on the seasonal cycle of the Antarctic sea-ice cover. *Climate Dyn.*, 15:251–268.

Fogli, P. G. and Coauthors (2009). INGV-CMCC Carbon (ICC): A carbon cycle earth system model. *CMCC Tech. Rep*, 61:30.

Garfinkel, C. and Hartmann, D. (2007). Effects of the El-Niño Southern Oscillation and the Quasi-Biennial Oscillation on polar temperatures in the stratosphere. *J.Geophys.Res.-Atmos.*, 112.

Garfinkel, C., Hartmann, D., and Sassi, F. (2010). Tropospheric precursors of anomalous northern hemisphere stratospheric polar vortices. *J.Clim.*, 23.

Garfinkel, C., Shaw, T., Hartmann, D., and Waugh, D. (2012). Does the Holton - Tan mechanism explain how the quasi-biennial oscillation modulates the Arctic polar vortex? *J. Atmos. Sci.*, 69:1713 – 1733.

Giorgetta, M., Manzini, E., Roeckner, E., Esch, M., and Bengtsson, L. (2006). Climatology and forcing of the quasi-biennial oscillation in the MAECHAM5 model. *J Clim*, 19:3882–3901.

Giorgetta, M. A. et al. (2013). Climate and carbon cycle changes from 1850 to 2100 in MPI-ESM simulations for the Coupled Model Intercomparison Project phase 5. *J. Adv. Model. Earth Syst.*, 5.

Goddard, L., Hurrell, J. W., Kirtman, B. P., Murphy, J., Stockdale, T., and Vera, C. (2012). Two time scales for the price of one (almost). *Bull. Amer. Meteor. Soc.*, 93:621-629.

Goddard, L., Kumar, A., Solomon, A.and Smith, D., Boer, G., Gonzalez, P., and ... & Delworth, T. (2013). A verification framework for interannual-to-decadal predictions experiments. *Climate Dynamics*, 40(1-2):245–272.

Goddard, L., Mason, S. J., Zebiak, S. E., Ropelewski, C. F., and Basher, R. & Cane, M. A. (2001). Current approaches to seasonal to interannual climate predictions. *International Journal of Climatology*, 21(9):1111–1152.

Gray, L., Crooks, S., Pascoe, C., Sparrow, S., and Palmer, M. (2004). Solar and QBO influences on the timing of stratospheric sudden warmings. *J. Atmos. Sci.*, 61(23):2777–2796.

Gray, L. and Pyle, J. (1989). A two-dimensional model of the quasi-biennial oscillation of ozone. *J. Atmos. Sci.*, 42:203–220.

Guemas, V., Corti, S., García-Serrano, J., Doblas-Reyes, F. J., Balmaseda, M., and Magnusson, L. (2013). The indian ocean: The region of highest skill worldwide in decadal climate prediction. *J. Climate*, 26:726–739.

Hamilton, K. (1984). Mean wind evolution through the quasi-biennial cycle in the tropical lower stratosphere. *J. Atmos. Sci.*, 47: 2113–2125.

Hamilton, K. (1998). Effects of an imposed quasi-biennial oscillation in a comprehensive troposphere - stratosphere - mesosphere general circulation model. *J. Atmos. Sci.*, 55:2393 – 2418.

Hampson, J. and Haynes, P. (2006). Influence of the Equatorial QBO on the Extratropical Stratosphere. *J. Atmos. Sci.*, 63:936–951.

Hawcroft, M. K., Shaffrey, L. C., Hodges, K. I., and Dacre, H. F. (2012). How much Northern Hemisphere precipitation is associated with extratropical cyclones? *Geophys. Res. Lett*, 39.

Hines, C. O. (1997). Doppler-spread parameterization of gravity- wave momentum deposition in the middle atmosphere. Part 1: Basic formulation. *J. Atmos. Sol. Terr. Phys.*, 59:371–386.

Hitchman, M.H. andHuesmann, A. (2002). Seasonal influence of the quasi-biennial oscillation on stratospheric jets and rossby wave breaking. *J.Atmos.Sci.*, 66:935–946.

Holton, J. R. and Tan, H. (1980). The Influence of the Equatorial Quasi-Biennial Oscillation on the Global Circulation at 50mb. *J. Atmos. Sci.*, 37:2200–2208.

Holton, J. R. and Tan, H. (1982). The quasi-biennial oscillation in the Northern Hemisphere lower stratosphere. *J. Meteor. Soc. Japan*, 60:140–148.

Hu, Y. and Tung, K. (2002). Tropospheric and equatorial influences on planetary-wave amplitude in the stratosphere. *Geophys.Res.Lett.*, 29(2):1019.

Hurrell, J. and Co-authors (2009). Decadal climate predictions: opportunities and challenges. *OceanObs '09 Community White Paper*, 1âĂŞ21.

Ilyina, T., Six, K. D., Segschneider, J., Maier-Reimer, E., Li, H., and Núñez-Riboni, I. (2013). The global ocean biogeochemistry model hamocc: Model architecture and performance as component of the mpi-earth system model in different cmip5 experimental realizations. *J. Adv. Model. Earth Syst.*

Ineson, S. and Scaife, A. (2009). The role of the stratosphere in the European climate response to El Niño. *Nature Geoscience*, 2(1):32–36.

Jolliffe, I. N. and Stephenson, D. B. (2003). Forecast verification. a practi-tionerâĂŹs guide in atmospheric science. *Wiley and Sons*, page 240.

Jungclaus, J. H. et al. (2006). Ocean Circulation and Tropical Variability in the Coupled Model ECHAM5/MPI-OM. *J. Climate*, 19:3952.

Jungclaus, J. H. et al. (2013). Characteristics of the ocean simulations in mpiom, the ocean component of the mpi-earth system model. *J. Adv. Model. Earth Syst.*

Kalnay, E. et al. (1996). The NCEP/NCAR 40-Year Reanalysis Project. *Bull. Amer. Meteor. Soc.*, 77:437–472.

Karin, L. (2005). On the solar cycle-QBO relationship: a summary. . *Journal of Atmospheric and Solar-Terrestrial Physics*, 67(1-2):45–54.

Keenlyside, N., Latif, M., Jungclaus, J., Kornblueh, L., and Roeckner, E. (2008). Advancing decadal-scale climate prediction in the north atlantic sector. *Nature*, 453:84–88.

Kim, H., Webster, P. J., and Curry, J. A. (2012). Evaluation of short-term climate change prediction in multi-model cmip5 decadal hindcasts. *Geophys. Res. Lett.*, 39.

Kinnersley, J. and Tung, K. (1999). Mechanisms for the extratropical QBO in circulation and ozone column. *J. Atmos. Sci.*, 56:1942–1962.

Kinnersley, J. and Tung, K. (2010). Equatorial quasi biennial oscillation influence on northern winter extratropical circulation. *J.Geophys.Res.*, 115.

Kodera, K. and Chiba, M. (1995). Tropospheric circulation changes associated with stratospheric sudden warmings: A case study. *J. Atmos. Sci*, 48(8): 1043–1061.

Kodera, K. and Koide, H. (1997). Spatial and seasonal characteristics of recent decadal trends in the northern hemispheric troposphere and stratosphere. *Journal of Geophysical Research*, 102.

Kodera, K. and Koide, H.and Yoshimura, H. (1999). Northern hemisphere winter circulation associated with the North Atlantic Oscillation and stratospheric polar-night jet. *Geophys.Res.Lett.*, 26:443–446.

Krismer, T. R., Giorgetta, M. A., , and Esch, M. (2013). Seasonal aspects of the quasibiennial oscillation in MPIESM and ERA40. *J. Adv. Model. Earth Syst*, 5(2) :406–421.

Kruschke, T., Rust, H., Kadow, C., Leckebusch, G., and Ulbrich, U. (2014). Evaluating decadal predictions of northern hemispheric cyclone frequencies. *Tellus A.*, 66:22830.

Kuroda, Y. (2008). Role of the stratosphere on the predictability of medium-range weather forecast: A case study of winter 2003-2004. *Geophys. Res. Lett.*, 35:L19701.

Labitzke, K. (1982). On the interannual variability of the middle stratosphere during the northern winters. *J. Meteor. Soc. Japan*, 60:124–139.

Latif, M. and Keenlyside, N. S. (2011). A perspective on decadal climate variability and predictability. *Deep-Sea Research II*, 10.1016.

Liu, Z. (2012). Dynamics of interdecadal climate variability: A historical perspective. *J. Climate*, 25:1963-1995.

Madec, G., Delecluse, P., Imbard, M., and Lvy, C. (1998). OPA 8.1 ocean general circulation model reference manual. Note du Pole de Modlisation 11. *Institut Pierre-Simon Laplace*, : 91.

Manzini, E., Cagnazzo, C., Fogli, P. G., Bellucci, A., and Müller, W. A. (2012). Stratosphere-troposphere coupling at inter-decadal time scales: Implications for the north atlantic ocean. *Geophys. Res. Lett.*, 39:L05801.

Manzini, E., Giorgetta, M., Esch, M., Kornblueh, L., and Roeckner, E. (2006). The in uence of sea surface tem- peratures on the northern winter stratosphere: Ensemble simulations with the MAECHAM5 model. *J. Climate*, 19(16).

Marshall, A. and Scaife, A. (2010). Improved predictability of stratospheric sudden warming events in an atmospheric general circulation model with enhanced stratospheric resolution. *Journal of Geophysical Research*, 115.

Marshall, A. G. and Scaife, A. A. (2009). Impact of the QBO on surface winter climate. *J. Geophys. Res.*, 114.

Matei, D., Pohlmann, H., Jungclaus, J., Ḿuller, W., Haak, H., and Marotzke, J. (2013). Two tales of initializing decadal climate prediction experiments with the ECHAM5/MPI-OM model. *Journal of Climate*, 25:8502–8523.

Matsuno, T. (1970). Vertical propagation of stationary planetary waves in the winter Northern Hemisphere. *J. Atmos. Sci.*, 27:871–883.

Matsuno, T. (1971). A Dynamical Model of the Stratospheric Sudden Warming. *J. Atmospheric Sci.*, 28:1479–1494.

McPhaden, M. J. and Co-authors (1998). The Tropical Ocean Global Atmosphere observing system: A decade of progress. *J. Geophy. Res.*, 103:14169–14240.

Meehl, G., Goddard, L., Boer, G., Burgman, R., Br anstator, G., and Coauthors (2013). Decadal climate prediction: Un update from the trenches. *American Meteorological Society*.

Meehl, G. A., Goddard, L., Boer, G., Burgman, R., Branstator, G., and Coauthors (2014). Decadal climate prediction: an update from the trenches. *Bull. Am. Meteorol. Soc.*, 95(2):243-267.

Meehl, G. A., Goddard, L., Murphy, J., Stouffer, R. J., Boer, G., and Coauthors (2009). Decadal prediction: can it be skillful? *Bull. Am. Meteorol. Soc.*, 90(10):1467-1485.

Mitchell, D., Charlton-Perez, A., and Gray, L. (2011). Characterising the variability and extremes of the strato- spheric polar vortices using 2D moments. *J. Atmos. Sci.*, 68):1194–1213.

Moss et al. (2008). Report from the ipcc expert meeting towards new scenarios, held in noordwijkerhout the netherlands, in september, 2007. `http://www.ipcc.ch/scoping_meeting_ar5/expert-meeting-report-scenarios.pdf`.

Müller, W. A., Baehr, J., Haak, H., Jungclaus, J. H., Kröger, J., and Coauthors (2012). Forecast skill of multi-year seasonal means in the decadal prediction system of the max planck institute for meteorology. *Geophys. Res. Lett.*, 39:L22707.

Murphy, A. H. (1988). Skill scores based on the mean square error and their relationships to the correlation coefficient. *Mon. Wea. Rev.*, 116:2417-2424.

Naito, Y. and Yoden, S. (2006). Behavior of planetary waves before and after stratospheric sudden warmings events in several phases of the equa- torial QBO. *J. Atmos. Sci.*, 63:1637–1649.

Naujokat, B. (1986). An update of the observed quasi-biennial oscillation of the stratospheric winds over the Tropics. *J. Atmos. Sci.*, 43:1873–1877.

Niwano, M. and Takahashi, M. (1998). The influence of the equatorial qbo on the northern hemisphere winter circulation of agcm. *J.Meteorol.Soc.Jpn.*, 76:453.

Ortland, D. A., Skinner, W. R., Hays, P. B., Burrage, M. D., Lieberman, R. S., Marshall, A. R., and Gell, D. A. (1996). Measurements of stratospheric winds by the high resolution Doppler imager. *J. Geophys. Res.*, 101:10,351–10,363.

O'Sullivan, D. and Salby, M. L. (1990). Coupling of the quasi-biennial oscillation and the extratropical circulation in the stratosphere through planetary wave transport. *J. Atmos. Sci.*, 47:650.

O'Sullivan, D. and Young, R. (1992). Modeling the Quasi-biennial Oscillation's Effect on the Winter Stratospheric Circulation. *J. Atmos. Sci.*, 49:2437–2448.

Paredes, D., Trigo, R., García-Herrera, R., and Trigo, I. (2006). Understanding precipitation changes in iberia in early spring: weather typing and storm-tracking approaches. *J Hydrometeorol*, 7:101–113.

Pascoe, C. L. and Gray, L. J. and. Scaife, A. A. (2006). A GCM study of the influence of equatorial winds on the timing of sudden stratospheric warmings. *Geophys. Res. Lett.*, 33.

Pascoe, C. L., Gray, L. J., Crooks, S. A., Juckes, M. N., and Baldwin, M. P. (2005). The quasi-biennial oscilation: Analysis using ERA-40 data. *J. Geophys. Res.*, 110.

Pfahl, S. and Wernli, H. (2012). Quantifying the relevance of cyclones for precipitation extremes. *J. Climate*, 25:6770–6780.

Pierce, D. W., Barnett, T. P., Tokmakian, R., Semtner, A., Maltrud, M., Lysne, J. A., and Craig, A. (2004). The ACPI Project, Element 1: Initializing a coupled climate model from observed conditions. *Clim. Change*, 62:13–28.

Plumb, R. A. (1985). On the three-dimensional propagation of stationary waves. *J. Atmos. Sci.*, 42: 217–229.

Pohlmann, H., Jungclaus, J. H., Kohl, A., Stammer, D., and Marotzke, J. (2009). Initializing decadal climate predictions with the gecco oceanic synthesis: Effects on the north atlantic. *J. Clim.*, 22:3926–3938.

Pohlmann, H., Müller, W. A., Kulkarni, K., Kameswarrao, M., Matei, D., and co authors (2013). Improved forecast skill in the tropics in the new MiKlip decadal climate predictions. *Geophys. Res. Lett.*, 40:5798–5802.

Raddatz, T. et al. (2007). Will the tropical land biosphere dominate the climatecarbon cycle feedback during the twenty- first century? *Climate Dynamics*, 29(6):565–574.

Raible, C. C. (2007). On the relation between extremes of midlatitude cyclones and the atmospheric circulation using ERA40. *Geophys. Res. Lett.*, 34.

Rayner, N. A., Parker, D. E., Horton, E. B., K., F. C., Alexander, L. V., Rowell, D. P., Kent, E. C., and Kaplan, A. (2003). Global analyses of sea surface temperature, sea ice, and night marine air temperature since the late nineteenth century. *J Geophys Res.*, 108(D14):4407.

Reichler, T., Kim, J., Manzini, E., and Kröger, J. (2012). A stratospheric connection to atlantic climate variability. *Nat. Geosci.*, 5:783-787.

Reichler, T., Kushner, P. J., and Polvani, L. M. (2007). The coupled stratosphere-troposphere response to impulsive forcing from the troposphere. *J. Atmos. Sci.*, 62: 3337–3352.

Roeckner, E., Bäuml, G.and Bonaventura, L., Brokopf, R., Esch, M., Giorgetta, M., Hagemann, S., Kirchner, I., Kornblueh, L., Manzini, E., Rhodin, A., Schlese, U., Schulzweida, U., and Tompkins, A. (2003). The atmospheric general circulation model ECHAM5. Part I: Model description. *Max Planck Institute for Meteorology Rep*, pages 349, 127.

Roeckner, E., Brokopf, R., Esch, M., Giorgetta, M., Hagemann, S., Kornblueh, L., Manzini, E., Schlese, U., and Schulzweida, U. (2006). Sensitivity of simulated climate to horizontal and vertical resolution in the ECHAM5 atmosphere model. *J. Climate,*, 19:3771–791.

Ruzmaikin, A. andFeynman, J., Jiang, X., and .Yung, Y. (2005). Extratropical signature of the Quasi-Biennial Oscillation. *J.Geophys.Res.*, 110.

Sassi, F., Kinnison, D., Boville, B., Garcia, R., and Roble, R. (2004). Effect of El Niño Southern Oscillation on the dynamical, thermal, and chemical structure of the middle atmosphere. *J. Geophys. Res.*, 109(D17):1223–1238.

Scaife, A. A., Athanassiadou, M.and Andrews, M., Arribas, A., Baldwin, M., Dunstone, N., Knight, J., MacLachlan, C., Manzini, E., Müller, W. A., Pohlmann, H., Smith., D., Stockdale, T., and Williams, A. (2014). Predictability of the quasi-biennial oscillation and its northern winter teleconnection on seasonal to decadal timescales. *Geophys. Res. Lett.*, 41:1752–1758.

Scaife, A. A., Folland, C., Alexander, L., Moberg, A., and Knight, J. (2008). European climate extremes and the North Atlantic Oscillation. *J.Climate*, 21:72 – 83.

Scaife, A. A. and Knight, J. R. (2008). Ensemble simulations of the cold European winter of 2005-2006. *Q. J. R. Meteorol. Soc.*, 134:1647–1659.

Scherhag, R. (1952). Die explosionsartigen Stratosparenerwarmungen des Spatwinters 1952. *Ber Det Wetterdienstes US Zone*, 38:51–63.

Schimanke, S., Körper, J. K., Spangehl, T., and Cubasch, U. (2011). Multi-decadal variability of sudden stratospheric warmings in an aogcmt. *Geophys. Res. Lett.*, 38:L01801.

Schirber, S., Manzini, E., and Alexander, M. J. (2014). A convection-based gravity wave parameterization in a general circulation model: Implementation and improvements on the QBO. *J. Adv. Model. Earth Syst.*, 6:264–27.

Smith, D., Cusack, S., Colman, A., Folland, A., Harris, G., and Murphy, J. (2007). Improved surface temperature prediction for the coming decade from a global circulation model. *Science*, 317:796–799.

Smith, D. M., Eade, R., and Pohlmann, H. (2013). A comparison of full-field and anomaly initialization for seasonal to decadal climate prediction. *Clim. Dyn.*, 62:13–28.

Smith, K., Polvani, L., and Marsh, D. (2012). Mitigation of 21st century antarctic sea ice loss by stratospheric ozone recovery. *Geophysical Research Letters*, 39.

Solomon, A., Goddard, L., Kumar, A., Carton, J., Deser, C., and Coauthors (2011). Distinguishing the roles of natural and anthropogenically forced decadal climate variability. *Bull. Amer. Meteor. Soc*, 92:141-156.

Stevens, B. et al. (2013). The atmospheric component of the mpi-m earth system model: Echam6. *J. Adv. Model. Earth Syst.*, 5 (2):146–172.

Taylor, K. E., Stouffer, R. J., and Meehl, G. A. (2012). An overview of cmip5 and the experiment design. *Bull. Am. Meteorol. Soc.*, 93(4):485-498.

Thompson, D. W. J., Baldwin, M. P., and Wallace, J. M. (2002). Stratospheric Connection to Northern Hemisphere Wintertime Weather: Implications for Prediction. . *J. Clim.*, 15:1421–1428.

Tung, K. K. and Yang, H. (1994). Global QBO in Circulation and Ozone. Part II: A Simple Mechanistic Model. *J. Atmos. Sci.*, 51:2708–2721.

Uppala, S. M. (2005). The ERA-40 re-analysis. *Q.J.R. Meteorol. Soc.*, 131:2961–3012.

Valcke, S. E. (2006). OASIS3 user guide (prism 2-5). *PRISM-Support Initiative Rep*, 3:64.

van Oldenborgh, G. J., Doblas-Reyes, F. J., Wouters, B., and Hazeleger, W. (2012). Decadal prediction skill in a multi-model ensemble. *Clim.Dyn.*, 38:1263-1280.

Wang, C. and Picaut, J. (2004). Understanding ENSO physics -A review. In C. Wang, S.-P.Xie, J.Carton,Earth's Climate: The Ocean-Atmosphere Interaction. *American Geophysical Union*, 103:21–48.

Wilks, D. S. (2006a). Statistical methods in the atmospheric sciences. *International Geophysics Series*, 91.

Wilks, D. S. (2006b). *Statistical Methods in the Atmospheric Sciences*. Elsevier.

WMO (2002). Standardised verification system (SVS) for long-range forecasts (LRF). *Manual on the GDPS*, WMONo. 485:volume 1.

WMO (2010,2012). Manual on the global data-processing and forecasting system, volume i - global aspects. [updated in 2012]. `http://www.wmo.int/pages/prog/www/DPFS/documents/485_Vol_I_en_colour.pdf`.

Yamashita, Y., Akiyoshi, H., and Takahashi, M. (2011). Dynamical response in the northern hemisphere midlat- itude and high-latitude winter to the QBO simulated by CCSR/NIES CCM. *J. Geophys. Res.*, 116.

Acknowledgements

I am using this opportunity to express my gratitude to everyone who lived with me the course of my PhD studies.
I express my thanks to Alessio Bellucci and Chiara Cagnazzo for their bilateral guidance, important criticism, patient availability and friendly advice during the project work.
I would like to thank Holger Pohlmann and Elisa Manzini for sharing their truthful and illuminating views, giving helpful and novel ideas and showing high interest related to the project.
I express my warm thanks to Daniela Domeisen for our scientific discussions, friendship and her support that gave me the right philosophy to continue this adventure.
I greatly benefited of the energetic encouragement of Panos Athanasiadis for monitoring the advancement of this thesis.
I am sincerely grateful to Natalia Calvo and Stefano Tibaldi for thorough review and I highly appreciate the comments and suggestions, which significantly contributed to improving the quality of this thesis.
This research was jointly performed at Euro-Mediterranean Centre for Climate Change (CMCC) in Bologna and at Max Planck Institute for meteorology in Hamburg. I thank the Max Planck Institute for providing access to their MPI-ESM-MR decadal simulations and I'm grateful to Müller Wolfgang for supporting the work on this project.

Dedication

Ai miei compagni di viaggio...

Dopo aver consultato l'oracolo Vittoria, i due Saggi del paese decisero di accompagnarmi al porto per farmi iniziare questa nuova esperienza ...

Su una nave dispersa in mezzo all'oceano si può contare solo sulla forza dell'equipaggio, io ho potuto contare su quella miei compagni d'avventura :
Daniele che ha sopportato i miei mal di mare quotidiani; Ali che ha cercato di trasmettermi la sua calma senza successo; la ridondante presenza romana e "il porto con tre mosche" che insieme insegnano sempre a non prendere il "mal di mare" troppo sul serio.
Sin dall'inizio di questo viaggio ÃÍ stato un fidato membro dell'equipaggio, Damiano, sempre al mio fianco ad eseguire i "comandi" a bordo!
Non dimentico gli avventurieri di passaggio che con il loro bizzarro idioma hanno lasciato il segno; sono ripartiti per terre lontane e sconosciute, ma rimangono comunque vicini.
L'approdo in terra tedesca mi ha riservato una calorosa accoglienza e l'incontro di un'altra Miriam dalle mille energie.
Nell'ultima traversata nuovi membri dell'equipaggio hanno partecipato all'ormeggio.

Consegno il diario di bordo all'unica persona che può dare il giusto peso ad ogni singola parola, custodirne gelosamente il contenuto e regalargli, conoscendola, letture sempre nuove.

Vi porterò sempre con me.